

b138 519 .13

U.O.V.S. BIBLIOTEK

UOVS BIBLIOTEK- EN INLIGTINGSDIENS  
UOFS LIBRARY AND INFORMATION SERVICES

BLOEMFONTEIN

Besorg terug op:

Return on:

2003 -02- 10	2004 -02- 11
05 MAR 2003	
	29 MAR 2004
2003 -07- 14	12 AUG 2004
29 JUL 2003	
26 AUG 2003	
2003 -09- 29	
30 OCT 2003	
14 NOV 2003	
01 DEC 2003	
05 JAN 2004	

B9

NIE UITLEENBAAR VOOR  
2001 -06- 11

02

mb

B

University Free State



34300000425177

Universiteit Vrystaat

THE DETERMINATION OF TERNARY  
SEGREGATION PARAMETERS USING  
A LINEAR HEATING METHOD

J. K. O. ASANTE

# The Determination Of Ternary Segregation Parameters Using A Linear Heating Method

by

**Joseph Kwaku Ofori Asante**

**B.Sc Hons.**

*This dissertation is offered for the fulfilment of the requirements for the degree*

**MASTER OF SCIENCE**

*in the Department of Physics*

*Faculty of Science*

*at the University of the Orange Free State*

*in*

*Bloemfontein*

*Republic of South Africa*

**Study Leader: Dr. W. D. Roos**

**Co-study Leader: Prof. J. du Plessis**

November 2000

## ACKNOWLEDGEMENTS

The author wishes to express his sincere appreciation to the following people:

- *Almighty GOD*, for his expressed mandate to the author in Gen.1:28.
- *My wife: Ama, sons: Kofi and Kobby, daughters: Akosua and Nhyira*, for their encouragement and spiritual support in tackling work of this nature.
- *Dr. WD Roos*, the author's study leader, for his knowledge and great ideas in the field of this subject.
- *Prof. J du Plessis*, the author's co-study leader, for his expert advice on this subject.
- *Mr. JJ Terblans*, from the Department of Physics (UOFS), for his assistance in the running of the ternary computer programme.
- *Dr. MF Maritz*, from the Department of Physics (UOFS), for his assistance in the extraction of the true Auger yield for the overlapping segregates in the APPH quantification.
- *Prof. HC Swart*, from the Department of Physics (UOFS), for his assistance in the vapour deposition.
- *Prof. GLP Berning*, the Head of the Department of Physics (UOFS), for his concerns and interest in this subject.
- The personnel of the Department of Physics (UOFS), for their assistance and support.
- The personnel of the Division of Instrumentation (UOFS), for their assistance.
- The personnel of the Division of Electronics (UOFS), for their assistance.

## ABSTRACT

In this study the segregation behaviour of the ternary system Cu(111),Sb,Sn is investigated experimentally, as well as with the modified Darken segregation model. The model, which describes the kinetics as well as the equilibrium of segregation, had been used successfully in various studies of binary systems. A computer program based on this model was developed for ternary systems.

A Cu(111) single crystal was doped with low concentrations of 0.180 at% Sb and 0.133 at% Sn using evaporation and diffusion process. The experimental results were gathered with the Auger electron spectroscopy technique. This technique was combined with a linear temperature ramp that makes it possible to obtain the segregation parameters in a single run. The traditional method requires various runs at different temperatures.

The overlapping of Sb and Sn Auger peaks in the energy regions of interest necessitated the development of a method to successfully extract the true contributions of the elements from the measured spectra. It is clearly shown that the combination of Auger peaks is not linear and that the true contributions of Sb and Sn can be calculated if the peaks overlap in two energy regions and the standard spectra are available.

The segregation profiles resulted from the Auger data show clearly the sequential segregation of the two elements (Sn and Sb). From the equilibrium conditions, it is also concluded that an interaction energy between Sb and Sn is present. By simulating the experimental results, using the theoretical Darken model, values for the segregation parameters can be obtained. The initial values for the fits are found mathematically (high-energy regions) and manually (low energy regions). The calculated profiles fit the experimental results very well.

The present study confirms that Sn segregate first to the surface with  $D_o = 1.58 \times 10^{-5} \text{ m}^2 \text{ s}^{-1}$  and  $E = 170 \text{ kJ/mol}$ . Sb with a lower diffusion coefficient ( $D_o = 1.93 \times 10^{-8} \text{ m}^2 \text{ s}^{-1}$  and  $E = 150 \text{ kJ/mol}$ ) segregates at higher temperatures. A further increase in temperature results in the stronger segregate Sb, (with a higher segregation energy  $\Delta G = -74.6 \text{ kJ/mol}$ ) to displace the Sn ( $\Delta G = -59.0 \text{ kJ/mol}$ ) from the surface. From the simulations, it is clear that the maximum surface coverage for Sn is determined mainly by the attractive interaction ( $\Omega_{SnCu} = -8.25 \text{ kJ/mol}$ ) between Sn and Cu. The desegregation rate of Sn in this system is determined by the segregation rate of Sb. The segregation profile of Sb is similar to that in a binary system (Cu,Sb) with the desegregation rate of Sb much slower than the segregation rate. The study also shows definite attractive interaction between Sb and Cu ( $\Omega_{SbCu} = -17.05 \text{ kJ/mol}$ ) This trend was not observed in the studies of binary systems. There is, however, repulsive interaction between the segregates ( $\Omega_{SnSb} = 3.62 \text{ kJ/mol}$ ).

The repeatability of the segregation parameters at different heating rates shows that this experimental method can be used successfully.

# Contents

<b>1. INTRODUCTION</b>	<b>6</b>
1.1 Segregation phenomenon.....	6
1.2 The objectives of this work.....	10
1.3 The outline.....	10
<b>2. SEGREGATION THEORY</b>	<b>12</b>
2.1 Introduction.....	12
2.2 The Regular Solution Model for ternary alloys.....	13
2.3 The Modified Darken's model.....	15
2.3.1 The Darken rate equations for the ternary system.....	21
2.4 Guttman's ternary regular solution (TRS) model (Equilibrium segregation equations).....	25
2.5 Diffusion coefficient $D$ , and Mobility $M$ .....	27
2.6 Summary.....	28
<b>3 EXPERIMENTAL SETUP</b>	<b>29</b>
3.1 Introduction.....	29
3.2 The AES system.....	30
3.3 Sample Preparation.....	31
3.4 Sample mounting and cleaning.....	33
3.5 Linear Heating Method (Linear Temperature Ramp (LTR) runs).....	35
3.6 Constant Temperature run.....	36
<b>4 AES QUANTIFICATION AND PEAK OVERLAPPING</b>	<b>37</b>
4.1 Introduction.....	37
4.2 The inelastic mean free path, $\lambda$ .....	41

4.3 The back scattering term, $r_m$ .....	42
4.4 AES Quantification.....	44
4.5 Overlapping Auger peak-to-peak heights.....	45
4.6 Overlapping peaks of Sn and Sb.....	45
4.7 Method of extracting element true contribution to APPH.....	47
4.8 Correction of the segregation profiles.....	53
<b>5 RESULTS AND DISCUSSION</b>	<b>56</b>
5.1 Introduction.....	56
5.2 The true Sn and Sb contribution to the APPH.....	56
5.3 Fit Procedures.....	60
5.3.1 Determining the $\Omega_{ij}$ and $\Delta G_i$ values.....	60
5.3.2 Determining the $D_o$ and $E$ values.....	62
5.4 Auger spectra of the sample's surface.....	62
5.4.1 Before a LTR run.....	62
5.4.2 After a LTR run.....	63
5.5 Segregation profile divided into four regions.....	64
5.6 The segregation results of Sn and Sb in Cu(111).....	66
5.6.1 The LTR runs at the various heating rates.....	66
5.6.1.1 The LTR run at heating rate of 0.05 K/s.....	67
5.6.1.2 The LTR run at heating rate of 0.10 K/s.....	68
5.6.1.3 The LTR run at heating rate of 0.15 K/s.....	69
5.6.1.4 The LTR run at heating rate 0.20 K/s.....	70
5.6.2 A Constant Temperature Run at 400 °C.....	71
5.6.3 Summary of segregation parameters.....	73
5.7 A General Discussion.....	74
5.7.1 The segregation profiles for different heating rates.....	74
5.7.2 The influence of the interaction energies between the different atoms.....	76
5.7.2.1 Change in the interaction coefficient between Sn and Sb atoms ( $\Omega_{SnSb}$ ).....	76
5.7.2.2 Change in the interaction coefficient between Sn and Cu atoms ( $\Omega_{SnCu}$ ).....	77

5.7.2.3 Change in the interaction coefficient between Sb and Cu atoms ( $\Omega_{SbCu}$ ).....	78
5.8 Comparison to the Cu-Sn and Cu-Sb binary systems.....	79
5.9 Significance of the corrected APPH technique.....	81
<b>6 CONCLUSION</b>	<b>82</b>
6.1 What has evolved in the course of this work.....	84
6.2 Future work.....	85
<b>Appendix</b>	<b>86</b>
(A Matlab programme for APPH correction of overlapping peaks)	
<b>Bibliography</b>	<b>88</b>



# CHAPTER ONE

## INTRODUCTION

### 1.1 Segregation phenomenon

Segregation as a phenomenon, is an increase in the concentration of one or more of the components near lattice discontinuities or the surface in an alloy system. It is a thermally activated process and becomes significant at elevated temperatures. It is observable in the temperature range where the solubility limit is not exceeded [1].

Surface segregation then is commonly regarded as the redistribution of solute atoms between the surface and the bulk of a material resulting in a solute surface concentration which is generally higher than the solute bulk concentration. This redistribution comes about so that the total energy of the crystal is minimised [2]. When alloys are heated, the solute atoms, which are also the alloying elements, may move from thousands of layers inside the bulk toward the surface. By measuring these solute concentrations on the surface, their segregation parameters can be determined [3].

Gibbs [4] was the first scientist to treat surface segregation formally. The phenomenon is of great importance to the material and surface scientist. With the limited world natural

resources but growing demand of material (metallurgical) products, it is becoming imperative for material and surface science researchers to come out with proper understanding of each material's behaviour within its multi-parameter environment so that its best use could be defined. Most material products come in the form of alloys. The understanding and description of an alloy system would be possible if the segregation parameters of the individual alloying elements are known. From a metallurgical point of view, alloying elements could either be undesirable impurities or deliberate dopants in the alloying system. It is also becoming imperative to seek possible alternatives for elements with a limited or uncertain source. The factor of high cost and time of production of material products must also be decreased. With the increasing acquisition of segregation data on the various alloying elements, through surface and grain boundary segregation works, theoretical consideration and manufacturing of super alloys are becoming possible.

In the field of materials science and surface science, segregation of one or more components to interfaces and surfaces can influence both the physical and chemical properties of the alloy [5]. Indeed, segregation and co-segregation can induce the formation of two-dimension compounds at the surface [6-10]. This could be stabilised epitaxially and have different, better physical properties such as two-dimensional conductivity, superconductivity and magnetism compared to that of their individual constituents' [11]. At present, segregation investigations have been applied to many aspects, such as the study of brittle fracture [12]; grain-boundary diffusion and motion [13-15]. The environmental effects such as inter-granular corrosion and stress corrosion cracking [16]-[19], carburizing [20] and nitriding [21], the development of hardmetals [22]; especially in the catalytic field [23-24] are still being studied. The need to develop improved catalysts for use in connection with environmental protection and the creation of viable alternative energy systems have led to an increasing use of metal alloys as heterogeneous catalysts. Here, surface concentration plays a key role in controlling such important factors as activity and selectivity [25].

Surface segregation phenomenon is studied with surface sensitive techniques that can provide reliable information on both the structure and the composition of the segregated layer. In the present study, Auger electron spectroscopy (AES) is the surface technique used to monitor the concentration of the segregands as they reach the surface from deep inside the bulk with time or temperature.

McLean [26] was the first to derive an expression for the surface concentration of non-interacting segregating species. In multi-component alloys, however, several interaction mechanisms between the various alloying elements and impurities are possible. Guttman [27] proposed the first multi-component segregation theory in which provision is made for these interactions.

The models mentioned above, however, make use of thermodynamic theory and provide in the thermodynamic sense a description of the process without providing values for the segregation parameters such as the segregation energy, diffusion coefficient or mobility, interaction coefficient between the atoms and activation energy.

Much surface segregation work has already been done on binary alloys; segregation parameters of the alloying elements have been documented [28-32]. Though theory [33-34], accounting for segregation measurements in multi-component alloys abound, not much work has been done on such alloys. Besides, according to the literature, almost all the ternary alloy systems that have been considered are of the form  $M_s$ - $M_2$ - $N_m$ , where  $M_s$  is a metal substrate,  $M_2$  is a metal or semi-metal solute and  $N_m$  is a non-metal [35-37]. The few surface segregation studies in all-metal-ternary-alloy work that have been considered, however, focus on surface composition [37-38].

In the present all-metal-ternary-alloy work, the investigation is centred on the determination of segregation parameters of the solutes. This is the first of its kind. Again, it is also the first time that the technique of linear temperature ramp (LTR) is being used in an all-metal-ternary-alloy study.

For the special case of a ternary alloy, in which both solutes' composition are very small (less than 1 at%) as compared to the solvent, interaction between the atoms of the solutes could lead to either co-segregation or sequential segregation of the solutes. Attractive interaction between solute atoms lead to co-segregation, while repulsive interaction on the other hand, leads to sequential segregation or site competition [39-41].

The ternary alloy system, Cu-Sn-Sb, is called Britannia metal, a kind of pewter, depending on the atomic composition of the elements. Typically, it has 92% Sn, 6% Sb and 2% Cu [42]. Sheffield manufacturers first introduced the alloy in the late 18<sup>th</sup> century and it is a product of the Industrial Revolution. It is also known as "white metal". In the United States of America, Henry Ford used "babbitt", a 86% Sn, 7% Cu and 7% Sb alloy in the manufacturing of the bearings on his engines [43]. Already, and practically, bronze, the alloy of Cu and Sn, has been in existence for centuries. At present, in electronics, it is common practice to coat Cu alloy contacts with Sn, a process called "electrotinned" in order to minimise interface degradation [44]. It has also been found, however, that every tin plated Cu alloy experiences the formation of copper-tin intermetallic compounds ( $\text{Cu}_6\text{Sn}_5$  and  $\text{Cu}_3\text{Sn}$ ) at the interface of the tin and the base metal [45]. With time and/or increase in temperature, the intermetallic compound move towards the surface and can adversely affect contact resistance and solderability. The intermetallic growth could be retarded, however, by using a "barrier metal" (a metal that diffuses much, much more slowly with the base alloy and tin). Antimony could possibly serve as a "barrier metal".

The theoretical models for the present work are based on the Darken's rate equations, which were modified to incorporate the technique of Linear Temperature Ramp (LTR). LTR also known as linear programmed heating (LPH) was first applied to surface segregation measurements in 1992 by du Plessis and Viljoen [46]. The technique has since been used to determine the bulk diffusion coefficient of the segregating species in mainly binary alloys [40], [46] and only once in a N-S- $\alpha$  Fe ternary alloy [40].

## 1.2 The objectives of this work

The aims followed in this study were to:

1. Prepare a ternary single crystal Cu(111) with low concentrations of Sn and Sb.
2. Extend the modified Darken binary routine to accommodate ternary systems.
3. Measure the segregation behaviour of Sn and Sb in Cu(111) system using Auger electron spectroscopy and LTR.
4. Extract each segregate true contribution to Auger peak-to-peak height (APPH).
5. Extract the segregation parameters by fitting the theory to the experimental results.

## 1.3 The outline

This work is divided into chapters. In chapter 2, the segregation theory and models that are used to interpret experimental results are given. Mention is made of the Regular Solution Model followed by the Modified Darken's model that leads up to the Darken's rate equations for the ternary alloy system. Equilibrium segregation equations, under Guttman's Ternary Regular Solution (TRS) model are also highlighted. Finally, the relationship between diffusion coefficient and mobility is derived.

The surface measurement that the Auger Electron Spectroscopy (AES) gives, is the APPH. This must be quantified to molar fraction. Chapter 3 therefore deals with the AES

quantification. The overlapping of the peaks of tin and antimony and their influence on AES quantification is also discussed.

In chapter 4, the experimental set-up is given. Here, the sample preparation, apparatus and the experimental procedures are discussed. Also included in this chapter, is the procedure whereby segregation measurements were conducted.

Results and discussion follow in chapter 5. This includes all the experimental and theoretical data points in graphical form.

In Chapter 6 the final conclusions are made, a summary is given and future work is considered.

# CHAPTER TWO

## SEGREGATION THEORY

### 2.1 Introduction

A total description of surface segregation embraces both the kinetic and the equilibrium processes [47]. The phenomenon of surface segregation has been described as an uphill diffusion as far as concentration gradient is concerned [48]. From the kinetics of surface segregation, the diffusion parameters: diffusion coefficient  $D$ , pre-exponential factor  $D_0$ , mobility  $M$ , the activation energy  $E$ , interaction coefficient between the atoms  $i$  and  $j$ ,  $\Omega_{ij}$  and segregation energy  $\Delta G$ , could be extracted from the measured Auger electron spectroscopy (AES) intensity, the APPH [49]. The segregation energy  $\Delta G$ , is the extra driving force that enables the solute atoms to move to the surface, besides the concentration gradient [50]. A number of models [51-55] have been put forth to explain the segregation process.

In the following sections, the regular solution model by Guttman [56] that accounts for the interaction between the solute atoms, which provides an expression in the surface concentration for the activity coefficient; as well as the modified Darken theory that was used in this study, will be explained. Also explained will be Guttman's segregation equations and the relationship between mobility and the diffusion coefficient.

In all multi-component alloys the interactions between the atoms play an important role in the segregation process. Hildebrand [57], was the first to develop the regular solution model.

3

## 2.2 The Regular Solution Model for ternary alloys

2

Guttman[56] applied the regular solution model to account for the interactions in the surface segregation of ternary systems. The model is based on three assumptions:

1. Atoms are randomly distributed over positions in a three-dimensional lattice.
2. No vacancies exist.
3. The energy of the system may be expressed as the sum of pairwise interactions between neighbouring atoms.

The model proposes that the interaction coefficients  $\Omega_{ij}$ , in a regular solution, where the components have atomic concentrations  $X_i$ , are related to the excess free enthalpy  $G^E$ , and to the enthalpy of mixing  $H^M$  as [58];

$$G^E = H^M = \sum_{ij} \Omega_{ij} X_i X_j \quad (2.1)$$

For any multi-component alloy, the chemical potential  $\mu$  is given by

2  
2.2.1  
2



$$\mu_i^M = H_i^M + (1 - X_i) \left[ \frac{\partial H_i^M}{\partial X_i} \right] \quad (2.2)$$

Deducing from equation 2.1, the enthalpy of mixing  $H^M$  for the ternary system, (where,  $X_1 + X_2 + X_3 = 1$ ), is then given as:

$$H^M = \Omega_{12} X_1 X_2 + \Omega_{13} X_1 X_3 + \Omega_{23} X_2 X_3 \quad (2.3)$$

Substituting equation 2.3 into the ternary form of equation 2.2 and supposing purely substitutional behaviour for the alloy and eliminating the solvent concentration  $X_3$  yield the relationship between activity coefficients  $f_i$  and the interaction coefficients as:

$$H_1^M = RT \ln f_1 = \Omega_{13} (1 - X_1)^2 + \Omega_{23} X_2^2 + \Omega' X_2 (1 - X_1) \quad (2.4)$$

$$H_2^M = RT \ln f_2 = \Omega_{23} (1 - X_2)^2 + \Omega_{13} X_1^2 + \Omega' X_1 (1 - X_2) \quad (2.5)$$

$$H_3^M = RT \ln f_3 = \Omega_{13} X_1^2 + \Omega_{23} X_2^2 + \Omega' X_1 X_2 \quad (2.6)$$

where  $\Omega' = \Omega_{12} - \Omega_{13} - \Omega_{23}$ ,

$$RT \ln f_i = \mu_i - \mu_i^o - RT \ln X_i \quad [33],$$

and

$$\Omega_{ij} = -N_o Z [\epsilon_{ij} - (\epsilon_{ii} + \epsilon_{jj}) / 2]$$

where  $N_o$  is the Avogadro's number,  $Z$  is the co-ordination number in the crystal lattice, and  $\epsilon_{ij}$  is the interaction energy of an  $ij$  bond.

In the present work, Darken's model calculations are used to describe the experimental results for the segregation process. Another supportive model, also based on the regular solution model, but that accounts for the equilibrium part of the segregation process and developed by Guttman [59], for the ternary system, is also used in describing the experimental results.

## 2.3 The Modified Darken's model

This model considers the differences in the chemical potential as the driving force behind segregation [60-61]. Atoms will move from the bulk, a place of high chemical potential, to the surface, a place of low chemical potential.

The original model [62], proposes that the net flux of species  $i$  ( $J_i$ ) through a plane at  $x = b$  is given by:

$$J_i = -M_i C_i^{(b)} \left( \frac{\partial \mu_i}{\partial x} \right)_{x=b} \quad (2.7)$$

where  $C_i$  is the concentration of the species  $i$  in this plane and  $\mu_i$  is the chemical potential of the species  $i$ .  $M_i$  is called the mobility of the species  $i$ .

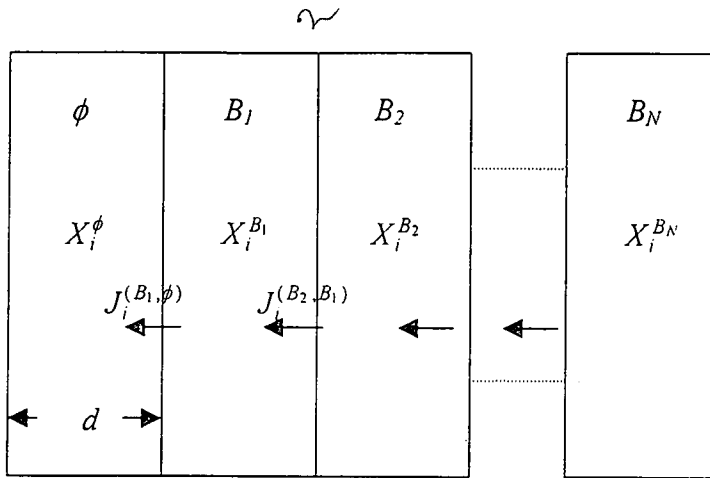


Figure 2.1 Division of the crystal into  $N + 1$  layers; the surface ( $\phi$ ) and bulk layers  $B_1 \rightarrow B_N$ .

If the crystal is divided into  $N + 1$  layers of thickness  $d$ , parallel to the surface, (see above figure 2.1), the Gibbs free energy of the two layers  $j$  and  $j + 1$  consisting of  $m$  components is given by:

$$G = \sum_{i=1}^m n_i^{(j)} \mu_i^{(j)} + \sum_{i=1}^m n_i^{(j+1)} \mu_i^{(j+1)} \quad (2.8)$$

where  $n_i^{(j)}$  is the number of moles of species  $i$  in the  $j$ -th layer and  $\mu_i^{(j)}$  is the chemical potential of the species  $i$  in the  $j$ -th layer.

The variation in the Gibbs free energy is expressed as:

$$\begin{aligned} \delta G &= \sum_{i=1}^m \left( \delta n_i^{(j)} \mu_i^{(j)} + n_i^{(j)} \delta \mu_i^{(j)} \right) + \sum_{i=1}^m \left( \delta n_i^{(j+1)} \mu_i^{(j+1)} + n_i^{(j+1)} \delta \mu_i^{(j+1)} \right) \\ &= \sum_{i=1}^m \left( \delta n_i^{(j)} \mu_i^{(j)} + \delta n_i^{(j+1)} \mu_i^{(j+1)} \right) \end{aligned} \quad (2.9)$$

(where  $n_i^{(j)} \partial \mu_i^{(j)} = 0$ , according to the Gibbs-Duhem equation [58]).

If atoms move from layer  $j + 1$  to layer  $j$ , then

$$\delta n_i^{(j)} = -\delta n_i^{(j+1)}$$

and equation 2.9 becomes

$$\delta G = \sum_{i=1}^m \delta n_i^{(j)} (\mu_i^{(j)} - \mu_i^{(j+1)}) \quad (2.10)$$

Also, if  $\delta n_i$  were independent, one would have

$$\frac{\partial G}{\partial n_i^{(j)}} = (\mu_i^{(j)} - \mu_i^{(j+1)}) \quad (2.11)$$

However, if the alloy is substitutional, the total number of moles in the layer is fixed, say  $n$ , and one obtains the following relations:

$$\sum_{i=1}^m n_i^{(j)} = n$$

which implies that

$$\sum_{i=1}^m \delta n_i^{(j)} = 0$$

that is,

$$\delta n_m^{(j)} + \sum_{i=1}^{m-1} \delta n_i^{(j)} = 0$$

and

$$\delta n_m^{(j)} = -\sum_{i=1}^{m-1} \delta n_i^{(j)}$$

Then equation 2.10 may be written as:

$$\delta G = \sum_{i=1}^{m-1} \delta n_i^{(j)} (\mu_i^{(j)} - \mu_i^{(j+1)}) + \delta n_m^{(j)} (\mu_m^{(j)} - \mu_m^{(j+1)})$$

$$= \sum_{i=1}^{m-1} \delta n_i^{(j)} (\mu_i^{(j)} - \mu_i^{(j+1)} - \mu_m^{(j)} + \mu_m^{(j+1)}) \quad (2.12)$$

from which it follows that

$$\frac{\partial G}{\partial n_i^{(j)}} = (\mu_i^{(j)} - \mu_i^{(j+1)} - \mu_m^{(j)} + \mu_m^{(j+1)}) \quad (2.13)$$

since all the summation, from 1 to  $m - 1$  terms, are independent. There are now two results: for a unrestricted layer and restricted (or substitutional) layer, given by equations 2.11 and 2.13 respectively.

If equations 2.7 and 2.11 are compared, one obtains

$$\frac{(\mu_i^{(j+1)} - \mu_i^{(j)})}{d} = \frac{-\partial G / \partial n_i^{(j)}}{d}$$

for a unrestricted layer, where the left hand side expression shows a decrease in  $G$  with  $n_i$ . The partial derivative implies that the driving force is the decrease in energy, and for an unrestricted layer, is given by:

$$\mu_i^{(j+1)} - \mu_i^{(j)}$$

and that for a substitutional layer:

$$\mu_i^{(j+1)} - \mu_i^{(j)} - \mu_m^{(j+1)} + \mu_m^{(j)}$$

Therefore the Darken flux equation can be modified [63] using;

$$\frac{\partial \mu_i}{\partial x} \rightarrow \frac{\Delta \mu_i^{(j+1,j)}}{d}$$

where

$$\Delta \mu_i^{(j+1,j)} = \left( \mu_i^{(j+1)} - \mu_i^{(j)} - \mu_m^{(j+1)} + \mu_m^{(j)} \right)$$

for substitutional alloys.

The flux of atoms from the  $(j + 1)$ -th layer to the  $j$ -th layer is then given by:

$$J_i^{(j+1,j)} = M_i C_i^{(j+1)} \frac{\Delta \mu_i^{(j+1,j)}}{d} \quad (2.14)$$

Further, if it is assumed that the net flux of atoms are moving towards the surface, then the rate of increase in the number  $N_i^{(j)}$  of species  $i$  in the  $j$ -th layer is given by:

$$\frac{\partial N_i^{(j)}}{\partial t} = d^2 \left( J_i^{(j+1,j)} - J_i^{(j,j-1)} \right) \quad (2.15)$$

which becomes, if both sides are divided by  $d^3$ ,

$$\frac{\partial C_i^{(j)}}{\partial t} = \frac{\left( J_i^{(j+1,j)} - J_i^{(j,j-1)} \right)}{d} \quad (2.16)$$

where  $C_i$  is the concentration of species  $i$  in the layer  $j$ .

If one considers the flux in the direction of the surface only, then another form of equation 2.14 gives

$$J_i^{(j,j-1)} = M_i C_i^{(j)} \frac{\Delta \mu_i^{(j,j-1)}}{d} \quad (2.17)$$

Substituting both equations 2.14 and 2.17 into equation 2.16 give

$$\frac{\partial C_i^{(j)}}{\partial t} = \left[ \frac{M_i C_i^{(j+1)}}{d^2} \Delta \mu_i^{(j+1,j)} - \frac{M_i C_i^{(j)}}{d^2} \Delta \mu_i^{(j,j-1)} \right]$$

Writing

$$C_i^{(j)} = X_i^{(j)} \frac{1}{d^3}$$

where  $X_i$  is the fractional concentration, one obtains

$$\frac{\partial X_i^{(j)}}{\partial t} = \left[ \frac{M_i X_i^{(j+1)}}{d^2} \Delta \mu_i^{(j+1,j)} - \frac{M_i X_i^{(j)}}{d^2} \Delta \mu_i^{(j,j-1)} \right] \quad (2.18)$$

Now there are  $(m-1)(N+1)$  rate equations for the  $N+1$  layers.

The segregation system of surface  $\phi$  and bulk  $B$  is therefore described by

$$\frac{\partial X_i^\phi}{\partial t} = \left[ \frac{M_i^{B_1 \rightarrow \phi} X_i^{B_1}}{d^2} \Delta \mu_i^{(B_1, \phi)} \right] \quad (2.19)$$

$$\frac{\partial X_i^{B_1}}{\partial t} = \left[ \frac{M_i^{B_2 \rightarrow B_1} X_i^{B_2}}{d^2} \Delta \mu_i^{(B_2, B_1)} - \frac{M_i^{B_1 \rightarrow \phi} X_i^{B_1}}{d^2} \Delta \mu_i^{(B_1, \phi)} \right] \quad (2.20)$$

$$\frac{\partial X_i^{(j)}}{\partial t} = \left[ \frac{M_i^{j+1 \rightarrow j} X_i^{(j+1)}}{d^2} \Delta \mu_i^{(j+1, j)} - \frac{M_i^{j \rightarrow j-1} X_i^{(j)}}{d^2} \Delta \mu_i^{(j, j-1)} \right] \quad (2.21)$$

for  $i = 1, 2, \dots, m - 1$  and  $j = \phi, B_1, \dots, B_N$ . Here  $X_i^\phi$  is the surface concentration,  $X_i^{B_1}$  is the first bulk layer concentration, and  $M_i$  is the mobility of species  $i$ .

### 2.3.1 The Darken rate equations for the ternary system

For the present ternary alloy,  $m = 3$ , that is, there are only two alloying species  $i = 1, 2$  besides the substrate. And there are two rate equations for each layer or cell of the crystal.

(a) The Rate Equations for the Surface Layer ( $\phi$ ) are given by:

$$\text{For solute 1,} \quad \frac{\partial X_1^\phi}{\partial t} = \left[ \frac{M_1^{B_1 \rightarrow \phi} X_1^{B_1}}{d^2} \Delta \mu_1^{(B_1, \phi)} \right] \quad (2.22)$$

$$\text{For solute 2,} \quad \frac{\partial X_2^\phi}{\partial t} = \left[ \frac{M_2^{B_1 \rightarrow \phi} X_2^{B_1}}{d^2} \Delta \mu_2^{(B_1, \phi)} \right] \quad (2.23)$$

According to the regular solution model,  $\Delta \mu_i^{(B_1, \phi)}$  is a function of both the segregation energies  $\Delta G_{ij}$  and the interaction parameters  $\Omega_{ij}$ , between the alloying elements or species.

Selecting the equations of solute 1 for further analysis, from equation 2.22, the difference in the chemical potential energy between the surface  $\phi$ , and the first bulk layer  $B_1$ ,  $\Delta \mu_1^{(B_1, \phi)}$ , is given by:



$$\Delta\mu_1^{(B_1, \phi)} = \mu_1^{B_1} - \mu_1^\phi + \mu_3^\phi - \mu_3^{B_1} \quad (2.24)$$

Expanding these chemical potential energy terms according to the regular solution model, equations 2.2 – 2.6, the following expressions for first bulk layer  $\mu^{B_1}$  and the surface layer  $\mu^\phi$  could be obtained:

$$\mu_1^{B_1} = \Omega_{13}(1 - X_1^{B_1})^2 + \Omega_{23}(X_2^{B_1})^2 + \Omega' X_2^{B_1}(1 - X_1^{B_1}) + RT \ln X_1^{B_1} \quad (2.25)$$

$$\mu_1^\phi = -\Delta G_1 + \Omega_{13} \left(1 - \frac{X_1^\phi}{X_1^{\phi M}}\right)^2 + \Omega_{23} \left(\frac{X_2^\phi}{X_2^{\phi M}}\right)^2 + \Omega' \frac{X_2^\phi}{X_2^{\phi M}} \left(1 - \frac{X_1^\phi}{X_1^{\phi M}}\right) + RT \ln \frac{X_1^\phi}{X_1^{\phi M}} \quad (2.26)$$

$$\mu_3^\phi = \Omega_{13} \left(\frac{X_1^\phi}{X_1^{\phi M}}\right)^2 + \Omega_{23} \left(\frac{X_2^\phi}{X_2^{\phi M}}\right)^2 - \Omega' \frac{X_1^\phi}{X_1^{\phi M}} \frac{X_2^\phi}{X_2^{\phi M}} + RT \ln \left(1 - \frac{X_1^\phi}{X_1^{\phi M}} - \frac{X_2^\phi}{X_2^{\phi M}}\right) \quad (2.27)$$

$$\mu_3^{B_1} = \Omega_{13}(X_1^{B_1})^2 + \Omega_{23}(X_2^{B_1})^2 - \Omega' X_1^{B_1} X_2^{B_1} + RT \ln(1 - X_1^{B_1} - X_2^{B_1}) \quad (2.28)$$

where  $X_i^{\phi M}$  is the maximum surface concentration of a segregate  $i$ .

Solute 2 (equation 2.23) also has similar expressions as equations 2.25 to 2.28, simply by writing subscript 2 in place of 1.

(b) The Rate Equations for the First Bulk layer,  $B_1$ , are:

$$\text{For solute 1, } \frac{\partial X_1^{B_1}}{\partial t} = \left[ \frac{M_1^{B_2 \rightarrow B_1} X_1^{B_2}}{d^2} \Delta \mu_1^{(B_2, B_1)} - \frac{\partial X_1^\phi}{\partial t} \right] \quad (2.29)$$

$$\text{For solute 2, } \frac{\partial X_2^{B_1}}{\partial t} = \left[ \frac{M_2^{B_2 \rightarrow B_1} X_2^{B_2}}{d^2} \Delta \mu_2^{(B_2, B_1)} - \frac{\partial X_2^\phi}{\partial t} \right] \quad (2.30)$$

Again from equation 2.29,

$$\Delta \mu_1^{(B_2, B_1)} = \mu_1^{B_2} - \mu_1^{B_1} + \mu_3^{B_1} - \mu_3^{B_2} \quad (2.31)$$

where

$$\mu_1^{B_2} = \Omega_{13}(1 - X_1^{B_2})^2 + \Omega_{23}(X_2^{B_2})^2 + \Omega' X_2^{B_2}(1 - X_1^{B_2}) + RT \ln X_1^{B_2} \quad (2.32)$$

$$\mu_1^{B_1} = \Omega_{13}(1 - X_1^{B_1})^2 + \Omega_{23}(X_2^{B_1})^2 + \Omega' X_2^{B_1}(1 - X_1^{B_1}) + RT \ln X_1^{B_1} \quad (2.33)$$

$$\mu_3^{B_1} = \Omega_{13}(X_1^{B_1})^2 + \Omega_{23}(X_2^{B_1})^2 - \Omega' X_1^{B_1} X_2^{B_1} + RT \ln(1 - X_1^{B_1} - X_2^{B_1}) \quad (2.34)$$

$$\mu_3^B = \Omega_{13}(X_1^{B_2})^2 + \Omega_{23}(X_2^{B_2})^2 - \Omega' X_1^{B_2} X_2^{B_2} + RT \ln(1 - X_1^{B_2} - X_2^{B_2}) \quad (2.35)$$

Again equations for solute 2 could be found from equation 2.30 by replacing subscript 1 in equations 2.31 up to 2.35 with 2.

## (c) Deeper Bulk layer rate equations

For the  $B_n$  layer, the concentration rates will be given by:

$$\text{For solute 1, } \frac{\partial X_1^{B_n}}{\partial t} = \left[ \frac{M_i^{B_{n+1} \rightarrow B_n} X_1^{B_{n-1}}}{d^2} \Delta \mu_1^{(B_{n+1}, B_n)} - \frac{\partial X_1^{B_{n-1}}}{\partial t} \right] \quad (2.36)$$

$$\text{For solute 2, } \frac{\partial X_2^{B_n}}{\partial t} = \left[ \frac{M_2^{B_{n+1} \rightarrow B_n} X_2^{B_{n+1}}}{d^2} \Delta \mu_2^{(B_{n+1}, B_n)} - \frac{\partial X_2^{B_{n-1}}}{\partial t} \right] \quad (2.37)$$

and

$$\Delta \mu_1^{(B_{n+1}, B_n)} = \mu_1^{B_{n+1}} - \mu_1^{B_n} + \mu_3^{B_n} - \mu_3^{B_{n+1}} \quad (2.38)$$

where

$$\mu_1^{B_{n+1}} = \Omega_{13}(1 - X_1^{B_{n+1}})^2 + \Omega_{23}(X_2^{B_{n+1}})^2 + \Omega' X_2^{B_{n+1}}(1 - X_1^{B_{n+1}}) + RT \ln X_1^{B_{n+1}} \quad (2.39)$$

$$\mu_1^{B_n} = \Omega_{13}(1 - X_1^{B_n})^2 + \Omega_{23}(X_2^{B_n})^2 + \Omega' X_2^{B_n}(1 - X_1^{B_n}) + RT \ln X_1^{B_n} \quad (2.40)$$

$$\mu_3^{B_n} = \Omega_{13}(X_1^{B_n})^2 + \Omega_{23}(X_2^{B_n})^2 - \Omega' X_1^{B_n} X_2^{B_n} + RT \ln(1 - X_1^{B_n} - X_2^{B_n}) \quad (2.41)$$

$$\mu_3^{B_{n+1}} = \Omega_{13}(X_1^{B_{n+1}})^2 + \Omega_{23}(X_2^{B_{n+1}})^2 - \Omega' X_1^{B_{n+1}} X_2^{B_{n+1}} + RT \ln(1 - X_1^{B_{n+1}} - X_2^{B_{n+1}}) \quad (2.42)$$

## (d) Final layer Rate Equations

Limiting the number of layers in which solute atoms segregate towards the surface as ninety nine in order to ease computational time as far as the solution of the differential

equations go, the rate contribution of the hundredth and the deeper layers could be considered zero. Thus,

$$\text{for solute 1,} \quad \frac{\partial X_1^{100}}{\partial t} = 0 \quad (2.43)$$

and

$$\text{for solute 2,} \quad \frac{\partial X_2^{100}}{\partial t} = 0 \quad (2.44)$$

All the coupled differential equations 2.22, 2.29...2.36 and 2.43 for the solute 1 are integrated whilst the equations of solute 2 are made constant. Also the time parameter,  $t$ , is converted to temperature,  $T$ , according to  $T = T_o + \alpha t$ , where  $T_o$  is the starting temperature and  $\alpha$  is the rate at which the sample is heated

## 2.4 Guttman's ternary regular solution (TRS) model (Equilibrium segregation equations)

From equation 2.13, equilibrium state would be reached when the Gibbs free energy is a minimum at constant temperature and pressure [63]. Thus,

$$\frac{\partial G}{\partial n_i^{(j)}} = 0$$

and the equilibrium conditions become:

$$\mu_i^\phi - \mu_i^B - \mu_m^\phi + \mu_m^B = 0 \quad (2.43)$$

For the ternary system, however,  $i = 1, 2$  and  $m = 3$  and the equilibrium equations, in terms of chemical potential terms, give:

$$\mu_1^\phi - \mu_1^B - \mu_3^\phi + \mu_3^B = 0 \quad (2.44)$$

$$\mu_2^\phi - \mu_2^B - \mu_3^\phi + \mu_3^B = 0 \quad (2.45)$$

Expanding each of the chemical potential terms, as before, using the regular solution equations 2.4 to 2.6 [58], the following segregation energy equations are obtained:

$$X_1^\phi = \frac{X_1^B \exp(\Delta G_1 / RT)}{1 - X_1^B + X_1^B \exp(\Delta G_1 / RT) - X_2^B + X_2^B \exp(\Delta G_2 / RT)} \quad (2.46)$$

$$X_2^\phi = \frac{X_2^B \exp(\Delta G_2 / RT)}{1 - X_1^B + X_1^B \exp(\Delta G_1 / RT) - X_2^B + X_2^B \exp(\Delta G_2 / RT)} \quad (2.47)$$

where

$$\Delta G_1 = \Delta G_1^0 + 2\Omega_{13}(X_1^B - X_1^\phi) + \Omega'(X_2^\phi - X_2^B) \quad (2.48)$$

$$\Delta G_2 = \Delta G_2^0 + 2\Omega_{23}(X_2^B - X_2^\phi) + \Omega'(X_1^\phi - X_1^B) \quad (2.49)$$

Equations 2.46 and 2.47 indicate that element  $i$  will segregate to the surface if  $\Delta G_i > 0$ .

Further, according to equations 2.48 and 2.49, there are three driving forces in the segregation energy  $\Delta G_i$ . The first is the difference in standard chemical potentials between the surface and the bulk ( $\Delta G_i^0$ ); the second is the term in  $\Omega_{i3}$  which could be called the

self-interaction term and lastly, the term  $\Omega'$  which takes into account the interactions between the solute atoms. The segregation energy  $\Delta G_i$  will thus be positive for  $\Omega_{i3} < 0$  and  $\Omega' > 0$ .

Equations 2.46 and 2.47 can be used to get the segregation energies  $\Delta G_i$  and the interaction coefficients  $\Omega_{ij}$  mathematically by fitting to the equilibrium (high temperature region) values of the measured data.

## 2.5 Diffusion coefficient $D$ , and Mobility $M$

From the two flux equations 2.7 and 2.14, Fick and Darken respectively, we have

$$-D_i \left( \frac{\partial C}{\partial x} \right)_{x=b} = J_i = -M_i C_i^{(b)} \left( \frac{\partial \mu_i}{\partial x} \right)_{x=b}$$

and therefore

$$D_i = M_i C_i^{(b)} \frac{\partial \mu_i}{\partial C_i}$$

or

$$D_i = M_i \frac{\partial \mu_i}{\partial \ln X_i} \quad (2.50)$$

where  $X_i$  is the fractional concentration and  $\partial C_i / C_i = \partial \ln X_i$

But, chemical potential energy  $\mu$ , is related to the atomic concentration  $X$ , according to [33],

$$\mu_i = \mu_i^0 + RT \ln f_i + RT \ln X_i$$

therefore

$$\frac{\partial \mu_i}{\partial \ln X_i} = RT \left( 1 + \frac{\partial \ln f_i}{\partial \ln X_i} \right)$$

and substituting into equation 2.43 we have

$$D_i = M_i RT \left( 1 + \frac{\partial \ln f_i}{\partial \ln X_i} \right) \quad (2.51)$$

In an ideal solution ( $f_i = 1$ ) or in a dilute solution ( $f_i = \text{constant}$ ) the derivative is zero, yielding

$$D_i = M_i RT \quad (2.52)$$

## 2.6 Summary

From the above discussion, the use of the equilibrium segregation equations helps in the mathematical determination of the segregation energies of the solutes as well as the interaction coefficients of all the alloying elements in the high temperature region of the experimental values. This, at this stage, means that the number of fitting values (segregation parameters) that are to be determined manually, in the solution of the Darken rate equations, are reduced only to diffusion coefficients and activation energies.

# CHAPTER THREE

## EXPERIMENTAL SETUP

### 3.1 Introduction

Sample preparation is a very important aspect of work of this nature. The outcome of the experiment is based totally on sample preparation. In this section, the Auger electron spectroscopy (AES) as a surface technique as well as the other apparatus used in the study will be discussed. An account of sample preparation and the experimental procedures that were followed will also be given.

The AES was developed in the late 1960's, deriving its name from the effect first observed by Pierre Auger, a French Physicist, in the mid-1920's [64]. It is based upon the measurement of the kinetic energies of the emitted Auger electrons. These Auger electrons are energy analysed and counted to yield a spectrum of the number of electrons as a function of energy [65]. Each element in a sample being studied will give rise to a characteristic spectrum of peaks at various kinetic energies.



### 3.2 The AES system

The spectrometer consists of the following components (see Figure 3.1 below)

1. PHI 18-085 electron gun and control unit for providing the primary electron beam. In this study, the primary electron beam energy and current were 4 keV and  $3.5 \mu\text{A}$  respectively.
2. The Perkin Elmer 20-070 scanning system control for obtaining an image of the sample.
3. PHI 25-110 single pass cylindrical mirror analyser (CMA) for electron energy analysis.
4. PHI 20-805 analyser control for the Auger signal with modulation amplitude of 2eV.

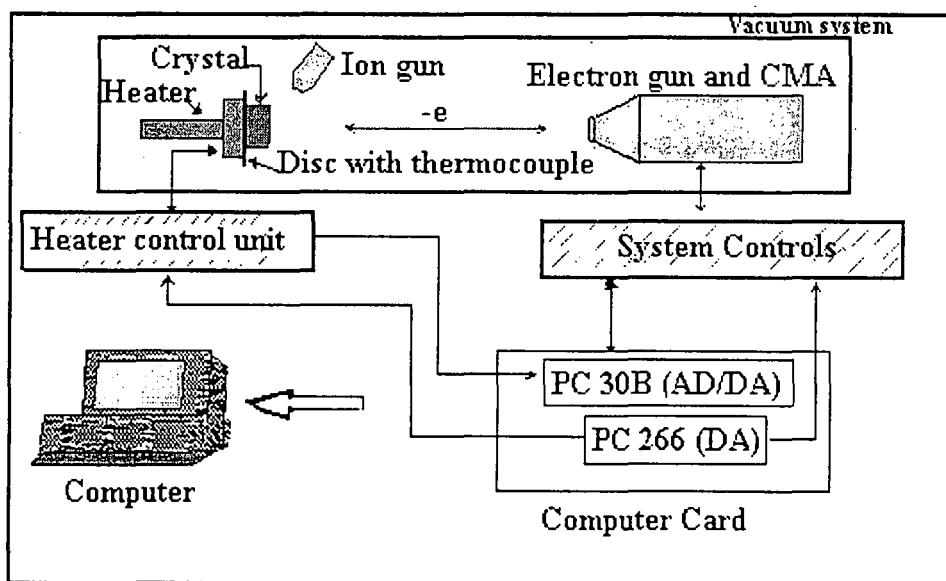


Figure 3.1 A diagram describing the AES system

5. PHI 32-010 Lock-in-amplifier differentiating the Auger signal with a sensitivity of 10mV and 0.3s time constant.

6. PHI 20-075 electron multiplier (high voltage supply) for providing high voltage to the electron multiplier inside the CMA. The voltage was 1800 V during measurements.
7. The Perkin Elmer 11-065 Ion gun control and the Perkin Elmer 04-303 differential Ion gun for cleaning the sample's surface. The ion beam current was approximately 30 nA as measured with a Faraday cup, and accelerating voltage of 2 keV. The argon gas pressure was  $2.0 \times 10^{-4}$  Pa.
8. A Varian 921-0066 ion pump and titanium sublimation pump maintaining a base pressure of less than  $2.0 \times 10^{-9}$  torr.
9. A Computer was used for controlling and data acquisitions.

### 3.3 Sample Preparation

A Cu single crystal, of 99.999 % purity and orientated to the (111) surface was ordered from Mateck, in Germany [66]. It was 6.58 mm in diameter and 0.63 mm thick. Polycrystalline Cu of 99.99 % purity and standards of Sb (purity 99.995 %) and Sn (purity 99.995 %) pellets, were obtained from Goodfellow Cambridge Limited [67]. The samples, which include six dummy Cu polycrystalline samples, were mechanically polished up to 1  $\mu$ m using a diamond suspended solution.

The single crystal and three dummy Cu samples were mounted side-by-side on a carousel and introduced into an evaporation chamber (see **Figure 3.2** below). A 33.5 k $\text{\AA}$  layer of Sb was evaporated onto the back, unpolished surface, of the samples by using an electron beam. The base pressure was  $10^{-7}$  torr.



### 3.4 Sample mounting and cleaning

The single Cu alloy was mounted onto a resistance heater as seen in **figure 3.3 (b)** below. A chromel-alumel thermocouple was spot-welded to a steel disc wedged between the heater and the back of the sample. The dummy polycrystalline alloy had chromel-alumel thermocouple junction pinched into its surface to determine the surface temperature as in **figure 3.3 (a)**. The surface temperature of the single Cu alloy was then calibrated against that of the dummy alloy.

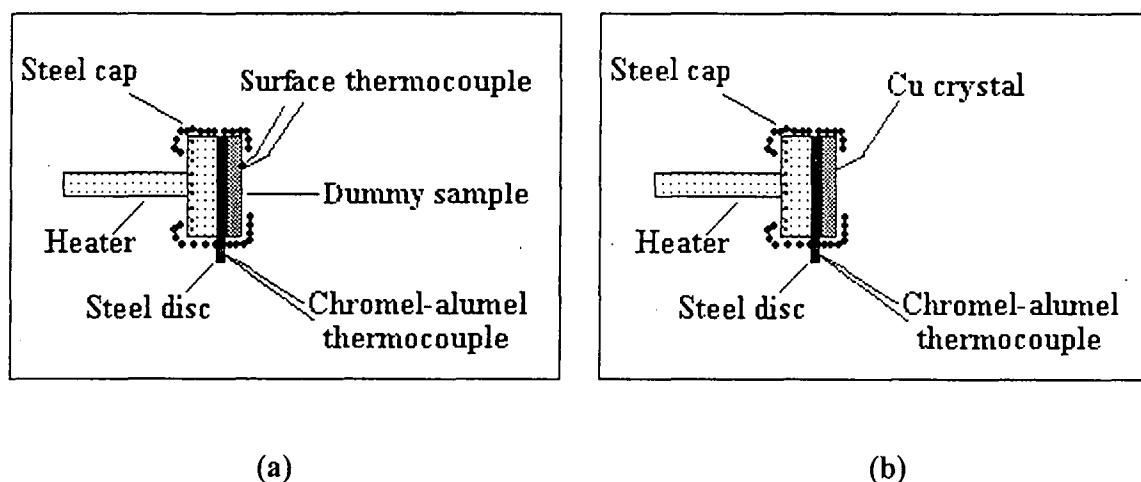


**Figure 3.3** Temperature measurement of the dummy (a) and the Single Cu crystal (b).

Mounted side-by-side to the ternary alloy, on the same carousel of the AES system, were standard samples of Cu, Sb and Sn (See **Figure 3.4** below).

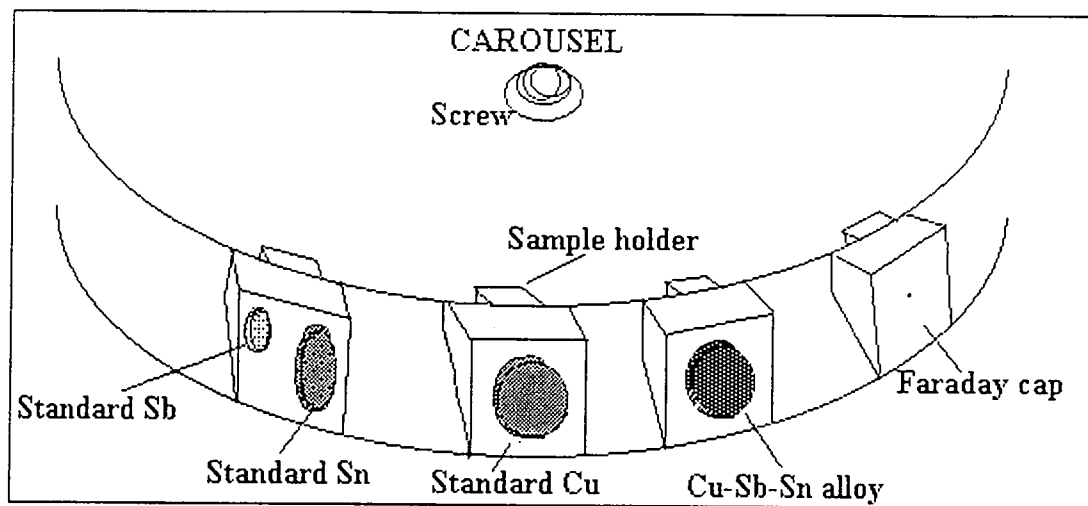


Figure 3.4 The arrangement of the crystals onto the carousel in the AES system

The AES spectra of these standards were used in the quantification (see Chapter 4).

Before the LTR runs, the sample was first cleaned of contaminants (C, S, O) by using the following procedure:

1. The sample was sputtered using 2 keV energy  $\text{Ar}^+$  ion bombardment and rastered over an area of 3 mm  $\times$  3 mm at room temperature for 10 minutes.
2. It was then heated to 550 °C and sputtered again for 5 minutes
3. It was further heated to 650 °C for 10 minutes without sputtering so as to level off any concentration gradient and also, to order the surface [69].
4. The sample was then cooled down to 550 °C and sputtered for 5 minutes.
5. The cycle (steps 2 and 3) were repeated four times, which resulted in a cleaned surface. (See Figure 5.5 in Chapter Five).

### 3.5 Linear Heating Method

#### (Linear Temperature Ramp (LTR) runs)

Since the early days of Surface Physics, the well-known square-root-of-time (SQR) solution of the diffusion equation (equation 3.1 below), have been used for the determination of bulk diffusion parameters via surface segregation [70-72].

$$X^{\phi} = X^B \left[ 1 + \frac{2}{d} \left( \frac{Dt}{\pi} \right)^{1/2} \right] \quad (3.1)$$

However, equation 3.1 is only valid for:

1. a constant diffusion coefficient,  $D$
2. a homogeneous bulk concentration at  $t = 0$  and
3. for short times.

There have been two methods for obtaining segregation measurements with SQR. In the first method, the surface of the sample is sputter-cleaned at room temperature. The temperature is then increased in steps to the desired temperature. The problem here is that diffusion can occur before the desired temperature is reached (the influence of finite heater response) and condition 1 is flouted. In the second method, the sample is first heated to the desired temperature and the surface sputter cleaned after thermal equilibrium has been reached. Segregation continues to take place whilst sample is being cleaned and result in a depleted region just below the surface. Condition 2 is therefore not fulfilled. Apart from these problems,  $D$  values have to be obtained at least at three temperatures for three different runs and it is difficult, if not impossible, to get exactly identical initial conditions for all measurements [73].

However, in heating the sample linearly at the rate of  $\alpha$  with time  $t$ , (see equation 3.2 below), the problems highlighted above are eliminated.

$$T = T_o + \alpha t \quad (3.2)$$

The sample surface is cleaned at room temperature, and at the start of the run ( $T_o$ ), as has been described in **section 3.4**, where sputtered-induced segregation and subsurface modification can be neglected. At low temperatures, according to [74], these modifications are restricted to the near surface region of  $\approx 10$  atomic layers. In addition, the linear heating method utilises a single experimental run in the range of temperatures that the sample is heated to.

In the LTR runs, the computer was programmed to start increasing the crystal temperature from 150 °C at a specified heating rate. The run was terminated at 630 °C. The heating rates considered were: 0.05 °C/s ; 0.10 °C/s , 0.15 °C/s and 0.20 °C/s.

An AES spectrum was taken at the end of a run, making sure that there were no other segregating elements except Sb and Sn (See **Figure 5.6**). After a run, the crystal was heated further to 650 °C and allowed at that temperature for 20 minutes to annul any concentration gradient.

### 3.6 Constant temperature run

There was one constant temperature run at 400 °C. For this run, the sample was heated quickly to 400 °C and was sputter-cleaned for a few seconds before the run. AES spectrum was taken at the end of a run and showed no segregating elements except Sn and Sb.

# CHAPTER FOUR

## AES QUANTIFICATION AND PEAK OVERLAPPING

### 4.1 Introduction

The conversion from APPH to molar fraction depends on a number of factors. Firstly, the APPH in the derivative mode of an element A is related to the atom density (in atoms/m<sup>3</sup>) of the element ( $N_A(z)$ ), at a depth  $z$  from the surface, besides other parameters as [69]:

$$I_A = I_o \sigma_A(E_o) [\sec \alpha(E_A)] R_m(E_A) T(E_A) D(E_A) \int_0^{\infty} N_A(z) \times \exp\left[-\frac{z}{\lambda_m(E_A) \cos \theta}\right] dz \quad (4.1)$$

where  $I_o$  is the primary electron current,  $\sigma_A(E_o)$  is the ionisation cross section of atom A by electrons with energy  $E_o$ ,  $\alpha$  is the angle of incidence of the primary electrons,  $R_m(E_A) = 1 + r_m(E_A)$  and  $r_m(E_A)$  is the back scattering term dependent on both the matrix  $m$



and the binding energy for the core level electron involved in the transition leading to an Auger electron with energy  $E_A$ ,  $T(E_A)$  is the transmission efficiency of the spectrometer,  $D(E_A)$  is the efficiency of the electron detector,  $\lambda_m(E_A)$  is the inelastic mean free path in the matrix  $m$  and  $\theta = 42^\circ$ , is the angle of emission.

In order to get a workable expression for a ternary alloy, the following assumptions are made:

- (1) the instrument factors;  $T(E_A)$  and  $D(E_A)$ , are assumed to be constant in the selected energy range.
- (2) The primary electron energy ( $E_o$ ), the angle of incidence of these electrons on the crystal ( $\alpha$ ) and the ionisation cross section that depend on  $E_o$ , ( $\sigma_A(E_o)$ ) are assumed constant.
- (3) The atomic densities are given by:

$$N_A^\infty = a_A^{-3} \quad (4.2)$$

$$N_A = X_A a_A^{-3} \quad (4.3)$$

where  $N_A^\infty$  is the atomic density of the pure element,  $N_A$  the atomic density of the element A in the matrix,  $a$  is the atom size and  $X_A$  is the mole fraction of element A. Thus equation 4.1 can be written as:

$$I_A = KR_m(E_A) \int_0^\infty \frac{X_A}{a_A^3} \times \exp\left[-\frac{z}{\lambda_m(E_A)\cos\theta}\right] dz \quad (4.4)$$

where

$$K = I_o \sigma_A(E_o) \sec \alpha(E_A) T(E_A) D(E_A)$$

The intensity for the pure element can then be written as:

$$\begin{aligned}
 I_A^\infty &= KR_\infty(E_A) \int_0^\infty \frac{1}{a_A^3} \times \exp\left[-\frac{z}{\lambda_\infty(E_A) \cos\theta}\right] dz \\
 &= \frac{KR_\infty(E_A)}{a_A^3} [\lambda_\infty(E_A) \cos\theta]
 \end{aligned}
 \tag{4.5}$$

From equation (4.5)

$$K = \frac{I_A^\infty a_A^3}{R_\infty(E_A) \lambda_\infty(E_A) \cos\theta}
 \tag{4.6}$$

If it is further assumed that the surface segregation of the element A covers a fraction of a mono-layer, with thickness,  $d_m$ , then equation 4.4 becomes after integration:

$$I_A = KR_m(E_A) \lambda_m(E_A) \cos\theta \frac{X_A^\phi}{a_A^3} \left[ 1 - \exp\left(-\frac{d_m}{\lambda_m(E_A) \cos\theta}\right) \right]
 \tag{4.7}$$

where  $X_A^\phi$  is the fractional surface coverage of element A.

Making  $X_A^\phi$  the subject of equation 4.7 gives:

$$X_A^\phi = \frac{I_A a_A^3}{KR_m(E_A) \lambda_m(E_A) \cos\theta} \left[ 1 - \exp\left(-\frac{d_m}{\lambda_m(E_A) \cos\theta}\right) \right]^{-1}
 \tag{4.8}$$

Finally, substituting for  $K$  (from equation 4.6) and cancelling out the inelastic mean free path for the pure element and that in the matrix, equation 4.8 yields:

$$X_A^\phi = \frac{I_A R_\infty(E_A)}{I_A^\infty R_m(E_A)} \left[ 1 - \exp\left(-\frac{d_m}{\lambda_m(E_A) \cos \theta}\right) \right]^{-1} \quad (4.9)$$

If there are more than one element on the surface, say B, the same is true for element B.

For the present ternary alloy sample, where Sb and Sn are of small concentrations in the Cu matrix, the following expressions hold for their fractional surface concentrations:

for Sn,

$$X_{Sn}^\phi = \frac{I_{Sn} R_\infty(E_{Sn})}{I_{Sn}^\infty R_{Cu}(E_{Sn})} \left[ 1 - \exp\left(-\frac{d_{av}}{\lambda_{Sn}(E_{Sn}) \cos \theta}\right) \right]^{-1} \quad (4.10)$$

for Sb,

$$X_{Sb}^\phi = \frac{I_{Sb} R_\infty(E_{Sb})}{I_{Sb}^\infty R_{Cu}(E_{Sb})} \left[ 1 - \exp\left(-\frac{d_{av}}{\lambda_{Sb}(E_{Sb}) \cos \theta}\right) \right]^{-1} \quad (4.11)$$

where  $d_{av}$  is the average size of Sn and Sb.

## 4.2 The inelastic mean free path, $\lambda$

From Powell [75]-[76], the inelastic mean free path (IMFP),  $\lambda$  in  $\text{\AA}$  is given by:

$$\lambda = E / \{E_p^2 [\beta \ln(\gamma E) - (C/E) + (D/E^2)]\} \quad (4.12)$$

where

$E$  is the electron energy in eV ,

$E_p = 28.8 (N_v \rho / M)^{1/2}$  is the free-electron plasmon energy in eV,

$\rho$  is the density in  $\text{gcm}^{-3}$ ,

$N_v$  is the number of valence electrons per atom (for elements) or molecule ( for compounds) and

$M$  is the atomic or molecular weight.

The terms  $\beta, \gamma, C$ , and  $D$  are adjustable parameters to the fits to the calculated IMFP and Tanuma [77] equate them to the following expressions:

$$\beta = -0.10 + 0.944 / (E_p^2 + E_g^2)^{1/2} + 0.069 \rho^{0.1} \quad (4.13)$$

$$\gamma = 0.191 \rho^{-0.50} \quad (4.14)$$

$$C = 1.97 - 0.91 U \quad (4.15)$$

$$D = 53.4 - 20.8 U \quad (4.16)$$

$$U = N_v \rho / M = E_p^2 / 829.4 \quad (4.17)$$

where  $E_g$  is the band-gap energy in eV for non-conductors.

The calculated IMFP for Sb (Auger electron with energy 460 eV) is:

$$\lambda_{\infty}(E_{Sb}) = 12.78 \text{ \AA}$$

The calculated IMFP for Sn (Auger electron with energy 433.5 eV) is:

$$\lambda_{\infty}(E_{Sn}) = 12.62 \text{ \AA}$$

### 4.3 The back scattering term, $r_m$

The back scattering term  $r_m$ , according to Shimizu [78]-[79], depends on the atomic number  $Z$  and the binding energy  $E_b$  of a particular element on the surface, and the primary electron energy  $E_o$ . It is given by:

$$r_m = (2.34 - 2.10 Z^{0.14}) \left( \frac{E_o}{E_b} \right)^{-0.35} + (2.58 Z^{0.14} - 2.98) \quad (4.18)$$

The back scattering term of Sn in the matrix,  $r_{Cu}(E_{Sn})$  is given by:

$$r_{Cu}(E_{Sn}) = (2.34 - 2.10 Z_{Cu}^{0.14}) \left( \frac{E_o}{E_{b(Sn)}} \right)^{-0.35} + (2.58 Z_{Cu}^{0.14} - 2.98) \quad (4.19)$$

where

$$Z_{Cu} = 29$$

$$E_o = 4000 \text{ V}$$

$E_{b(Sn)} = 485 \text{ eV}$  is the binding energy resulting in an Auger electron with energy 433.5 eV.

Thus,

$$r_{Cu}(E_{Sn}) = 0.664$$

For pure Sn, the back-scattering term,

$$r_{\infty}(E_{Sn}) = 0.864.$$

Similarly, the back scattering term of Sb in the matrix,  $r_{Cu}(E_{Sb})$  is given by:

$$r_{Cu}(E_{Sb}) = (2.34 - 2.10 Z_{Cu}^{0.14}) \left( \frac{E_o}{E_{b(Sb)}} \right)^{-0.35} + (2.58 Z_{Cu}^{0.14} - 2.98) \quad 4.20$$

where

$Z_{Cu} = 29$ , the atomic number for Cu

$E_o = 4000 \text{ V}$ , the primary electron energy

$E_{b(Sb)} = 528 \text{ eV}$ , is the binding energy resulting in an Auger electron with energy 460 eV. Thus,

$$r_{Cu}(E_{Sb}) = 0.649 \quad (4.21)$$

For pure Sb, the back scattering term,

$$r_{\infty}(E_{Sb}) = 0.853. \quad (4.22)$$

## 4.4 AES Quantification

Putting the necessary substitutions into equation 4.10, the final fractional concentration of Sn in terms of the APPH's values, ( $I_{Sn}$  in the alloy and  $I_{Sn}^{\infty}$  for the pure Sn) becomes:

$$X_{Sn}^{\phi} = \frac{I_{Sn}}{I_{Sn}^{\infty}} \times 3.86 \quad (4.23)$$

Similarly, the expression for Sb, from equation 4.11 gives:

$$X_{Sb}^{\phi} = \frac{I_{Sb}}{I_{Sb}^{\infty}} \times 3.92 \quad (4.24)$$

For each run, the APPH for the pure Sn and Sb are normalised against that of Cu for the particular heating rate.

However, because of the overlapping of peaks of Sb and Sn in the energy regions where their characteristic spectra are, the Auger contribution of each species in the measurement of the combined Auger peak-to-peak (APPH) must be resolved before the quantification of the APPH to surface fractional coverage can be completed. As a result, the measured APPH values  $I_{Sn}$  and  $I_{Sb}$  in equations 4.23 and 4.24 for Sn (426 – 440 eV) and Sb (450 – 463 eV) must still be corrected.

## 4.5 Overlapping Auger peak-to-peak heights

In the course of this work, a technique for extracting the Auger yield of each of two species with overlapping Auger peaks using only Auger peak-to-peak-heights (APPH's) of the derivative spectrum, that is,  $d(EN(E))/dE$  was developed. The need for this technique arises from the common practice to store only the APPH of a selected peak of each element that is studied during depth profiling or during a temperature run, instead of storing the full spectrum at each time step. The latter is often not done because sampling the full spectrum at each scan is considered too time consuming, and storing it requires too much memory. Some Auger apparatuses are capable of storing selected regions of the spectrum, and in this case, quantification of overlapping peaks can be done more accurately by means of decomposition of the combined peak into the spectra of the standards with a weighted least squares fit [80]. The number of independent species that contribute to a peak is determined by using factor analysis [81]. However, the presentation below is useful for quantifying data sampled with an apparatus that can only record either the full spectrum or a set of APPH's in selected energy ranges [82]. Even if the selected energy regions for the individual species for which the APPH is to be measured are very large, this technique can still be used to correct the APPH.

## 4.6 Overlapping peaks of Sn and Sb

In the present work, where sequential segregation of Sn and Sb in Cu(111) was observed (see Chapter Five), the Auger peaks of Sn and Sb standards were found to be overlapping in the energy range of 380-470 eV (see figure 4.1)



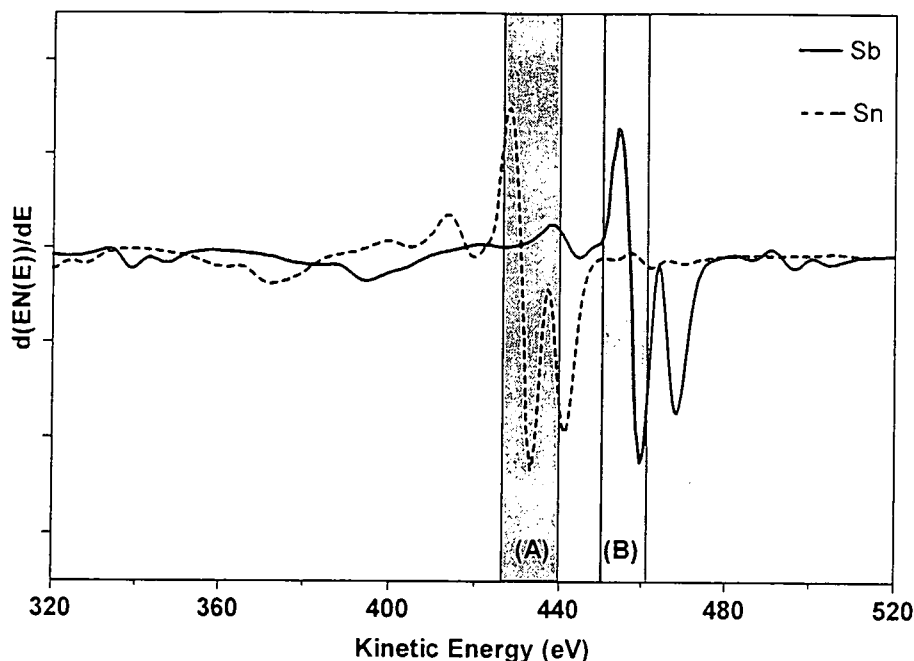


Figure 4.1 Overlapping of Sn and Sb peaks.

Although interval (A) contains a large Sn peak and small Sb contribution, and likewise interval (B) contains a large Sb peak together with a small Sn contribution, these small contributions do influence the APPH measurements and must be considered in the quantification procedure. This complicates the quantification of each species. Computer in the multiplexing mode recorded the APPH measurements. The cylindrical mirror analyser (CMA) voltage was scanned at a rate of 2 eV/s over the selected energy intervals consecutively and only the largest peak-to-peak height of the spectrum over each selected energy interval was recorded as a function of time. Thus, the APPH of the sum of two spectra peaks is not the linear sum of the APPH's of the two individual spectra, but the APPH of the higher peak.

The following energy region intervals were selected:

Interval (A): for Sn: 426 – 440 eV

Interval (B): for Sb: 450 – 463 eV

Interval (C): for Cu: 915 – 930 eV

Spectra of Sn, Sb and Cu standards were also obtained under the same experimental conditions.

## 4.7. Method of extracting element true contribution to APPH

The condition that must be fulfilled in this method lies in the choice of any two-energy interval (1) and (2) that must have some features of both elements.

In figure 4.2, two energy regions (1) and (2) are chosen as 385-420 eV and 437-458 eV respectively.

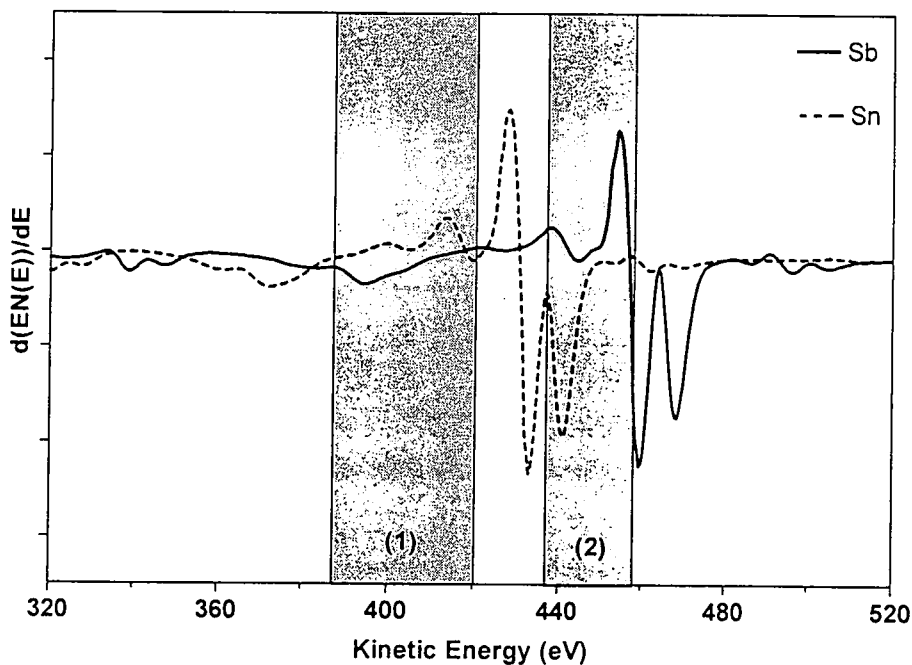


Figure 4.2 Two energy regions (1) and (2) of Auger spectra of Sn and Sb standards

The APPH function can be defined as:

$$\text{Apph}_{(X)}(f) = \max f(E) - \min f(E), \text{ for } E \in X$$

where  $f(E)$  is the derivative Auger spectrum given by:

$$f(E) = \frac{d(EN(E))}{dE} \quad (4.25)$$

and the prefix 'max' and 'min' standing for maximum and minimum of the function at a particular energy  $E$  within the energy interval  $X$  respectively and  $N(E)$  is the normal Auger spectrum.

If the derivative Auger peaks of two species P and Q overlap and the yield due to the former species is  $\alpha$  and the latter  $\beta$ , then their combined spectrum add linearly in the same energy interval as:

$$\alpha f_P(E) + \beta f_Q(E).$$

However, the APPH of the sum of the two spectra is not the sum of the APPH's of the two individual spectra. Although the first condition of linearity is satisfied, that is,

$$\text{Apph}_{(X)}(\alpha f) = \alpha \text{Apph}_{(X)}(f), \quad (4.26)$$

the second condition is violated, that is,

$$\text{Apph}_{(X)}(f_P + f_Q) \neq \text{Apph}_{(X)}(f_P) + \text{Apph}_{(X)}(f_Q) \quad (4.27)$$

Figure 4.3 illustrates this with a simple artificial example where:

$$\text{Apph}_{(X)}(f_P + f_Q) = \text{Apph}_{(X)}(f_P), \text{ in spite of the fact that } \text{Apph}_{(X)}(f_Q) \neq 0.$$

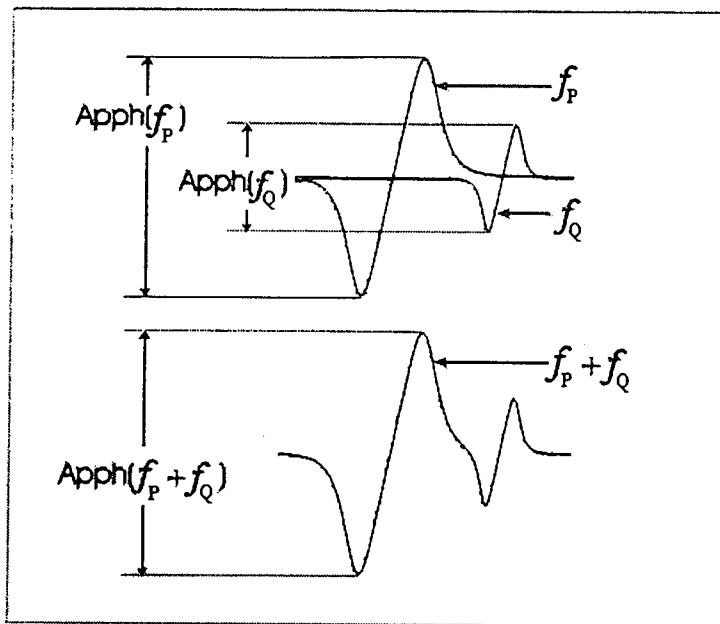


Figure 4.3 An example illustrating the non-linearity of the Apph function

The derivative Auger spectrum of Sn can then be taken as:

$$f_{Sn}(E) = \frac{d(EN_{Sn}(E))}{dE} \quad (4.28)$$

and that of Sb,

$$f_{Sb}(E) = \frac{d(EN_{Sb}(E))}{dE} \quad (4.29)$$

where  $N_{Sn}(E)$  and  $N_{Sb}(E)$  are the normal spectra of the Sn and Sb standards respectively. The APPH-functions of the combined peaks in the two energy intervals could also be defined as:

$$I_{(1)}(\alpha, \beta) = \text{Apph}_{(1)}(\alpha f_{Sn} + \beta f_{Sb}) \quad (4.30)$$

$$I_{(2)}(\alpha, \beta) = \text{Apph}_{(2)}(\alpha f_{Sn} + \beta f_{Sb}) \quad (4.31)$$

where  $\alpha$  and  $\beta$  are the true yield of Sn and Sb respectively in the APPH. Also, the subscripts (1) and (2) denote the two energy intervals where peaks overlap.  $I_{(1)}$  and  $I_{(2)}$  are not functions with known mathematical expressions. Each has to be evaluated computationally in the following way: it combines the spectra of the standards in the specified region using weights  $\alpha$  and  $\beta$ , then finds the maximum and minimum of the combination computationally and supplies the difference between the maximum and minimum as output.

The non-linearity of both  $I_{(1)}$  and  $I_{(2)}$  functions are clearly illustrated in the mesh diagrams and contour plots shown in Figure 4.4.1 (a), (b) and Figure 4.4.2 (c) and (d).

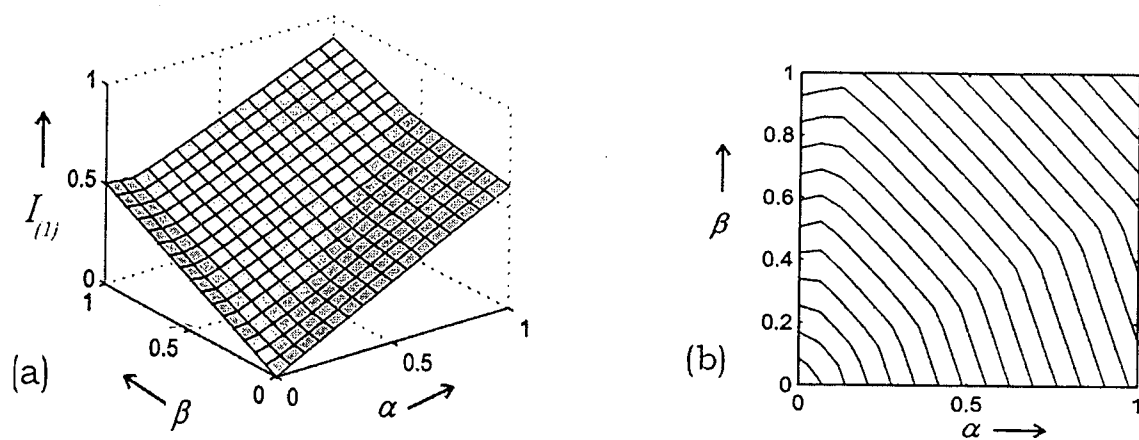


Figure 4.4.1 A mesh plot (a) and a contour plot (b) of  $I_{(1)}(\alpha, \beta)$

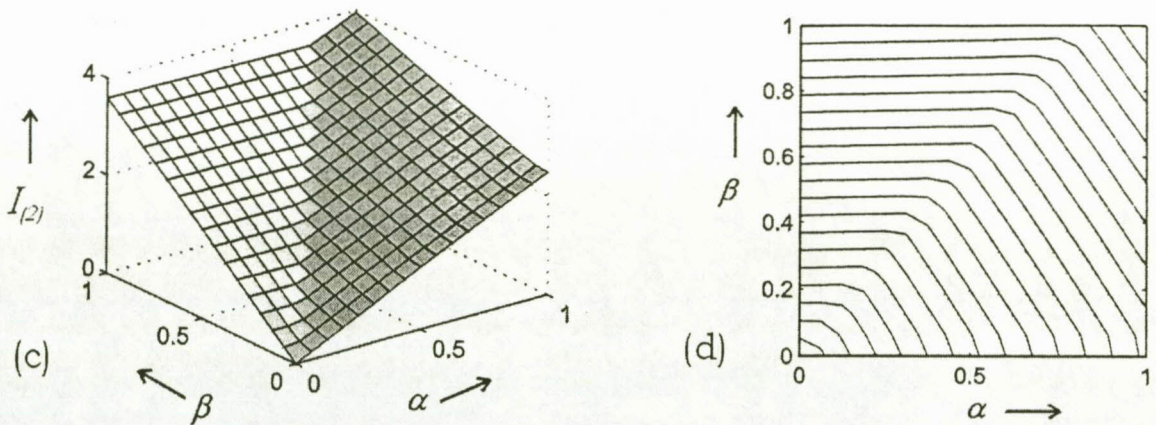


Figure 4.4.2 A mesh plot (c) and a contour plot (d) of  $I_{(2)}(\alpha, \beta)$

If the measured APPH's in energy intervals (1) and (2) are  $I_{(1)}^{me}$  and  $I_{(2)}^{me}$  respectively, then the simultaneous solution of:

$$I_{(1)}(\alpha, \beta) = I_{(1)}^{me} \quad (4.32)$$

and

$$I_{(2)}(\alpha, \beta) = I_{(2)}^{me} \quad (4.33)$$

yields the solution  $(\alpha, \beta)$ , where  $\alpha$  and  $\beta$  are the Auger contribution of Sn and Sb to the combined spectrum respectively.

Since equations 4.32 and 4.33 are non-linear in  $\alpha$  and  $\beta$ , a non-linear solution method of MATLAB's `fmins` function [83] type is used. The `fmins` function is based on the Nelder-Mead simplex algorithm. It requires a starting estimate of  $(\alpha, \beta)$  from which it commences its search for the minimum of the given function. In the present application, `fmins` was used to minimise:

$$g(\alpha, \beta) = [I_{(1)}(\alpha, \beta) - I_{(1)}^{me}]^2 + [I_{(2)}(\alpha, \beta) - I_{(2)}^{me}]^2 \tag{4.34}$$

with respect to  $\alpha$  and  $\beta$ . There may be more than two solutions for the non-linear equations 4.32 and 4.33. This is illustrated in **Figure 4.5**, which shows an overlay of the two contour plots.

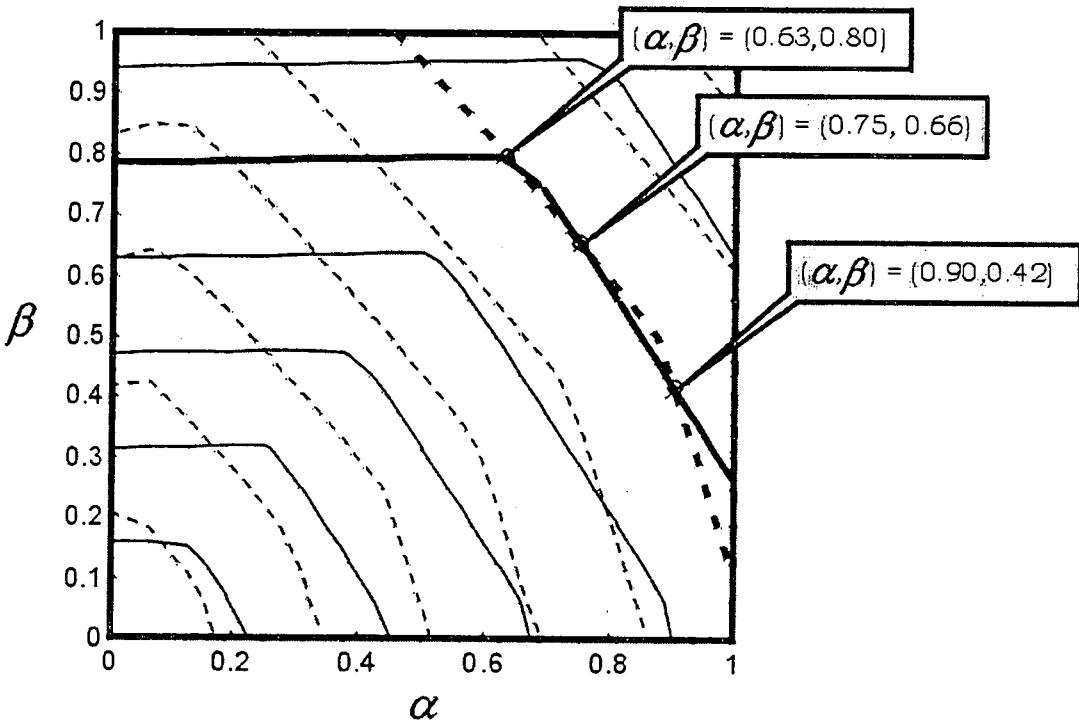


**Figure 4.5** An overlay contour plots of  $I_{(1)}(\alpha, \beta)$  (dashed) and  $I_{(2)}(\alpha, \beta)$  (solid) showing the contour  $I_{(1)} = 0.630$  as thicker dashed line and the contour  $I_{(2)} = 2.815$  as a thicker solid line. The three possible solutions are also shown.

Choosing, as a particular example,

$$I_{(1)}^{me} = 0.630 \text{ and } I_{(2)}^{me} = 2.815, \tag{4.35}$$

the solutions lie in the intersection of the contours; the contour  $I_{(1)}^{me} = 0.630$  is shown in a thicker dotted line in **Figure 4.5**, and the contour  $I_{(2)}^{me} = 2.815$  is shown in a thicker solid line.

From the intersection of the contours, it is clear that for this particular case, there are three solutions in the positive quadrant. The fmins search algorithm finds the solution  $(\alpha, \beta) = (0.6312, 0.7984)$  when for example  $(0, 0)$  is chosen as starting estimate. Similarly,  $(0.7488, 0.6567)$  is found with starting estimate  $(1, 1)$ , and  $(0.9014, 0.4203)$  with starting estimate  $(1, 0.3)$ . In depth profiling runs or temperature runs, the peaks do not change abruptly from one time step to the next and it is therefore suggested that the solution at the previous time step be used as starting estimate for solving the next step.

## 4.8 Correction of the segregation profiles

The APPH's of the standards for Sn and Sb in the intervals (A) and (B) above, can be expressed as  $I_{(A)}(1, 0)$  for the Sn standard and  $I_{(B)}(0, 1)$  for the Sb standard.

During the temperature run,  $I_{(A)}^{me}$  and  $I_{(B)}^{me}$  are sampled repeatedly, and are hence functions of time, therefore the two functions appropriately become;  $I_{(A)}^{me}(t)$  and  $I_{(B)}^{me}(t)$ . Although  $I_{(A)}^{me}(t)$  and  $I_{(B)}^{me}(t)$  are never sampled at the same instant  $t$ , the difference in consecutive sampling times is less than 20 seconds and therefore the sampling over both intervals can be taken as the mean of the two times.

A coarse method of quantification would be to consider interval (A) to contain only the Sn peak and interval (B) to contain only the Sb peak. In that case, the contribution of Sn to the Auger yield, disregarding the effect of the small contribution of the Sb part of the spectrum present in the interval (A) will be given by:



$$\bar{\alpha}(t) = \frac{I_{(A)}^{me}(t)}{I_{(A)}(1,0)} \quad (4.36)$$

Similarly, the contribution of Sb to the Auger yield, disregarding the effect of the small contribution of the Sn part of the spectrum in the interval (B) will be given by:

$$\bar{\beta}(t) = \frac{I_{(B)}^{me}(t)}{I_{(B)}(0,1)} \quad (4.37)$$

Equations 4.36 and 4.37 are synonyms to the right hand side of equations 4.23 and 4.24 respectively.

In order to find the correct contributions, however, a similar kind of equation 4.34 should be minimised with respect to  $\alpha$  and  $\beta$  for each value of  $t$ . Thus:

$$g(\alpha, \beta, t) = [I_{(A)}(\alpha, \beta) - I_{(A)}^{me}(t)]^2 + [I_{(B)}(\alpha, \beta) - I_{(B)}^{me}(t)]^2 \quad (4.38)$$

The solution is denoted by  $\alpha(t)$  and  $\beta(t)$ . The physical interpretation of this solution is that  $\alpha(t)$  is the contribution of Sn and  $\beta(t)$  the contribution of Sb to the relevant APPH's in the two separate intervals.

The starting estimate for each minimisation at time  $t$  is simply the solution of the previous time step. This choice of starting values ensures that the physically correct solution will be found in those instances where multiple solutions may be possible.

The MATLAB code for the script file which loops through all the time steps and calculates the correct contributions, together with two functions addressed in the above, is given in Appendix A.

It is to be noted that  $\alpha$  and  $\beta$  are still only 'contributions to the yield' and are not atomic fractions, since back-scattering effects and concentration profiles still have to be taken into account.

Finally, the correct Auger signal quantification becomes:

for Sn (from equation 4.23, the molar fraction in terms of the corrected APPH signal) gives:

$$X_{Sn}^{\phi} = \alpha(t) \times 3.86 \quad (4.39)$$

and similarly for Sb (from equation 4.24) gives:

$$X_{Sb}^{\phi} = \beta(t) \times 3.92 \quad (4.40)$$

The difference in corrected and uncorrected quantification is further shown in **Chapter 5 (Figure 5.3)**.

# CHAPTER FIVE

## RESULTS AND DISCUSSION

### 5.1 Introduction

In this chapter, the consequences of bad energy range selection on the APPH profiles are shown as well as the corrections made.

The fit procedure for the Darken model is also explained. In the later part of the chapter, the segregation profiles as well as the segregation parameters for the best fits are presented and discussed.

### 5.2 The true Sn and Sb contribution to the APPH

In Chapter Four, mention was made of peaks overlapping in the two energy regions where the APPH of Sn (426-440 eV) and Sb (450-463 eV) were determined with the

computer in the multiplex mode. The computer can not account for the influence of the lower Sb peak in the Sn energy range and the lower Sn peak in the Sb energy region during the APPH measurements. The true contributions of the two elements in the APPH measurements were extracted by the technique explained in the previous chapter.

A segregation profile using the chosen energy regions for Sn (400-440 eV) and Sb (440-480 eV) is presented below in **Figure 5.1**

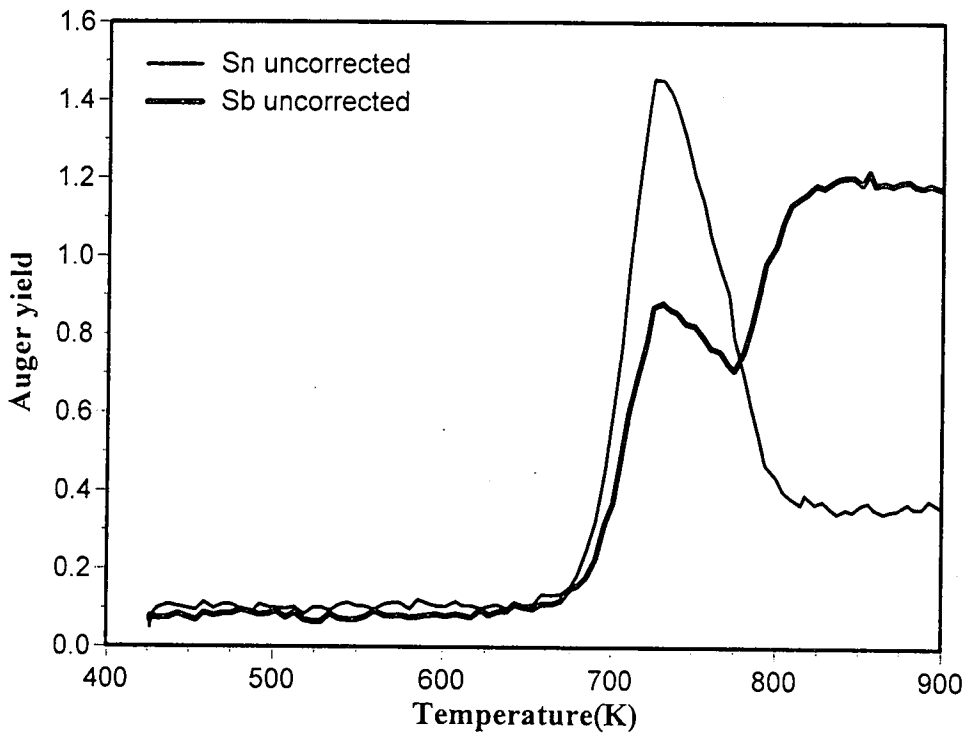


**Figure 5.1** Segregation profile of Sn and Sb where APPH measurements were taken for large energy regions with overlapping peaks.

It is clear from **Figure 5.1** that the profile of Sb in the temperature region 700 K to 800 K is very strange and not compatible to what is expected from the segregation theory described in Chapter Two. The reason for this unusual profile is an experimental one, and in particular the selections of energy regions used in determining the APPH as a function

of temperature. In the energy regions mentioned above, the Sn and Sb peaks overlap and one can thus expect the peaks to influence each other.

Even in the above case of “bad” energy region selection, the mathematical technique discussed in Chapter Four could be employed to extract the true Auger yield of each segregate. The requirements are:

1. the two energy regions have overlapping Auger peaks, and that
2. the standard Auger spectra under the same experimental conditions of the segregates should be available.

The figure below (**Figure 5.2**) shows the measured (or uncorrected) and corrected Auger yields for Sn and Sb for the same large energy interval as in **Figure 5.1** using the technique described in Chapter Four.

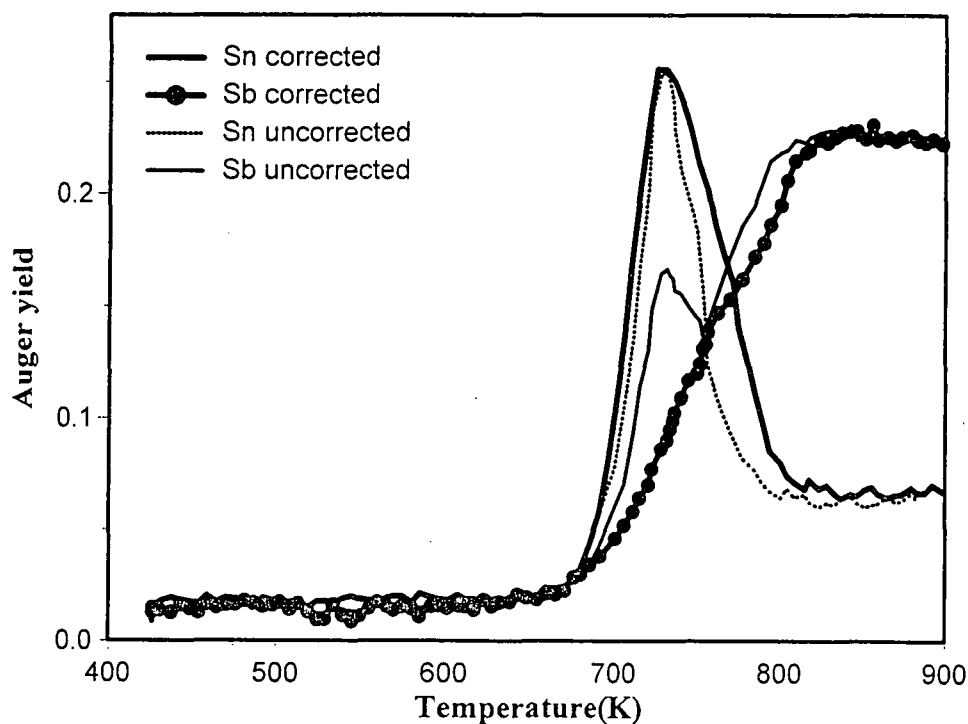


**Figure 5.2** The measured (or uncorrected) and corrected APPH segregation profiles of Sn and Sb. The energy regions for the APPH measurements of the segregates were large and therefore not a “good” choice.

Thus, in any multi-component alloy system where there might be overlapping of peaks of the segregates, the true contribution of each element to the combined measured APPH can be extracted to enable an accurate surface fraction quantification to be made.

The result of a better choice in energy regions, Sn (426-440 eV and Sb (450-463 eV) is given in Figure 5.3 below. The result is termed the corrected APPH segregation profile. In Figure 5.3, the corrected and measured (uncorrected) segregation profiles are given.

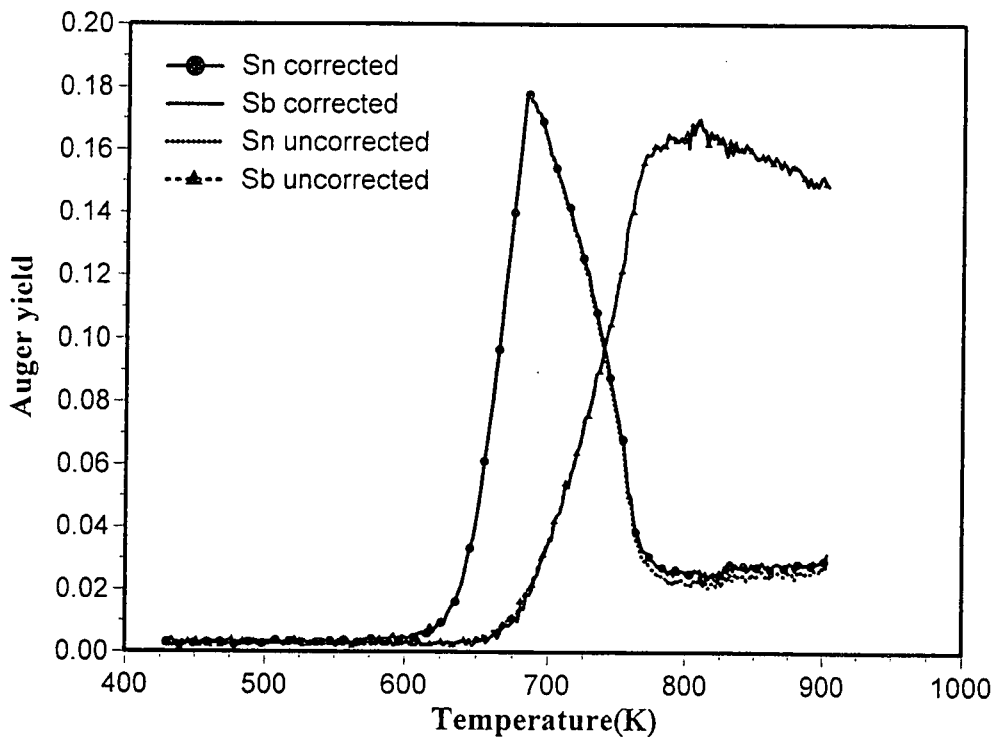


Figure 5.3 Segregation profiles of Sn and Sb in a LTR run at 0.1 K/s

It is to be expected that both the corrected and measured (uncorrected) Sn Auger yields will largely coincide in the energy region where Sn APPH is to be measured (426-440 eV) since this region contains a large Sn peak (refer to Figure 4.1). Similar expectations hold true for corrected and uncorrected Sb Auger yields in the energy region 450-463 eV. However, there are deviations between the corrected and the uncorrected curves. These

occur at those instances where the contribution of a predominant element to an interval (such as Sn in energy region 426-440 eV) is small while the contribution of the less important element to that interval (such as Sb to interval 426-440 eV) is large. These differences are seen (though not very pronounced) in the Sb curves between 675-720 K, and in the Sn curves at temperatures higher than 775 K. This implies that the energy intervals for the APPH measurements were "good" choices.

The rest of the segregation profiles were all corrected for the influence of overlapping peaks.

## 5.3 Fit Procedures

The fit procedure was carried out in two steps. Firstly, the interaction energies ( $\Omega_{ij}$ ) and the segregation energies ( $\Delta G_i$ ) were determined mathematically. Secondly, the diffusion parameters; the pre-exponential factor ( $D_{oi}$ ) and activation energies ( $E_i$ ), were determined manually.

### 5.3.1 Determining the $\Omega_{ij}$ and $\Delta G_i$ values

The following steps were used in determining the interaction parameters and segregation energies:

1. Equilibrium segregation equations 2.46 to 2.49 were used.
2. From the measured segregation profiles a temperature  $T_b$  was selected. This temperature is part of the high temperatures in the equilibrium coverage regions.
3. The MATLAB `fmins` function was used to determine the parameters, by minimising the function  $R$  that is the difference between the calculated and measured values in the temperature range  $T_b$  to  $T_e$ . The temperature,  $T_e$ , is the final temperature measured. See **Figure 5.4**.

$$R = \sum_{i=T_b}^{T_e} \{ (co(1) - cc(1,i))^2 + (co(2) - cc(2,i))^2 \} \quad (5.1)$$

Here,  $co$  is the calculated surface coverage and  $cc(n,i)$  is the measured surface coverage at temperature  $i$ . The numbers 1 and 2 refer to Sn and Sb respectively.

Finding values for the  $\Omega$ 's and  $\Delta G$ 's to best fit the measured values, is obtained by minimising  $R$ . This procedure can only be used for equilibrium coverage regions and is therefore applied on the high temperature side of the LTR profile, between  $T_b$  and  $T_e$ .

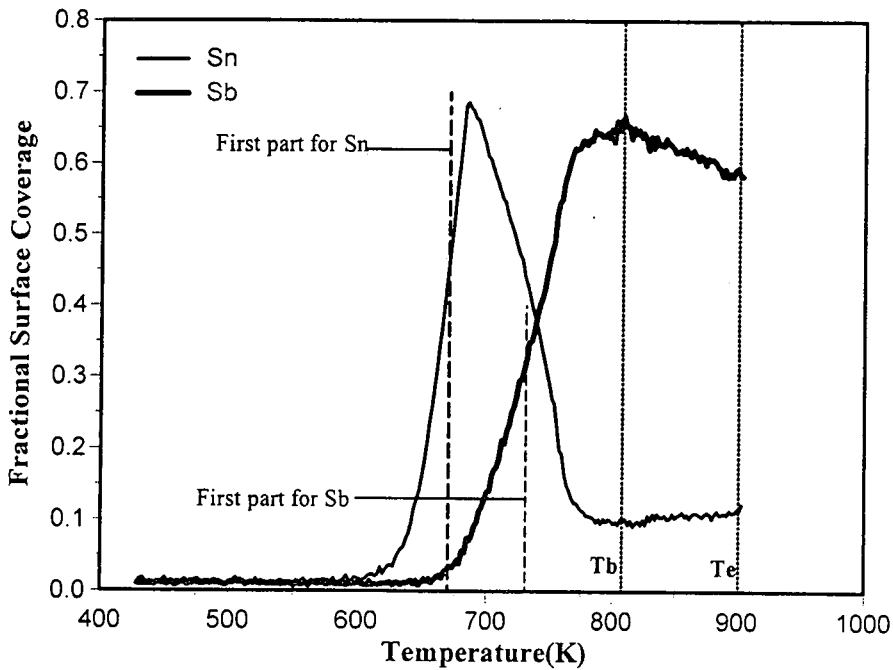


Figure 5.4 Segregation profiles for Sn and Sb. Changing  $D_o$  and  $E$  manually enables one to have the fit for the first part of Sn and Sb profiles as shown in the figure. The beginning temperature,  $T_b$ , as well as the final temperature,  $T_e$ , in the equilibrium regions are also shown.



### 5.3.2 Determining the $D_o$ and $E$ values.

These values were determined manually by using starting values for  $D_o$  and  $E$  determined previously for the binary systems [28] and [84]. These values were changed until a best fit, judged by eye, was obtained in the first part of the segregation profiles. See **Figure 5.4**.

## 5.4 Auger spectra of the sample's surface.

### 5.4.1 Before a LTR run

As indicated in the previous chapter, Auger spectra of the sample were taken after cleaning; just before a run. The figure below, **Figure 5.5**, shows one such spectrum. Only the characteristic peaks of Cu is detected and it implies that the surface of the sample is devoid of any other element except Cu atoms.

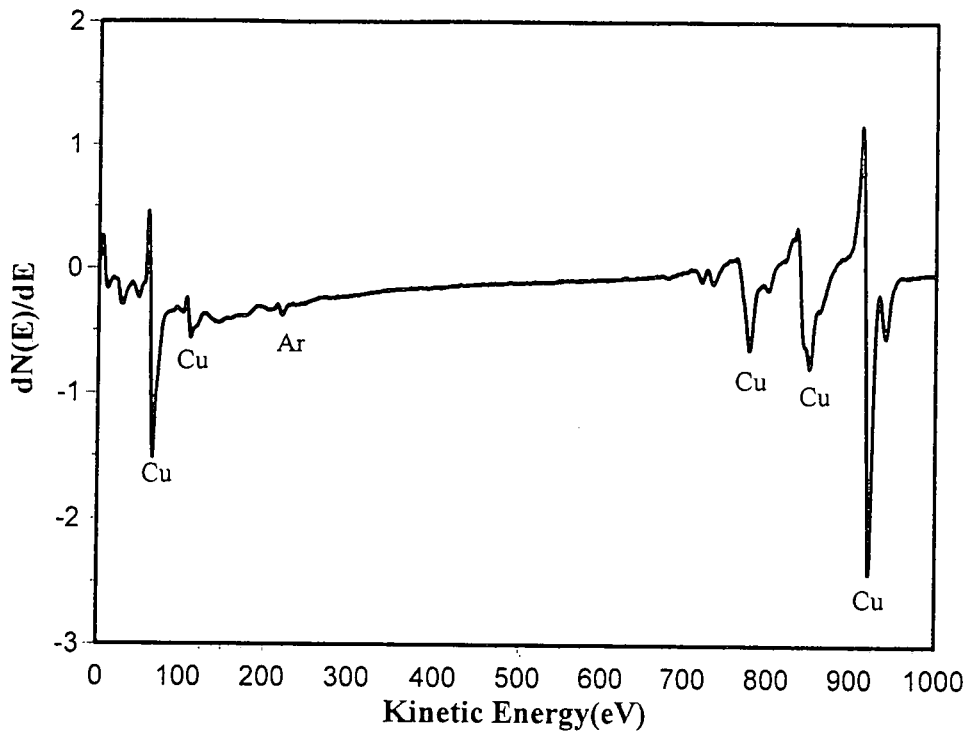


Figure 5.5 A typical Auger spectrum of the sample at 150 °C, taken after sputtering the surface, and just before a LTR run.

### 5.4.2 After a LTR run

Figure 5.6 below shows an Auger spectrum after a run. It is clear that no contaminants are present.

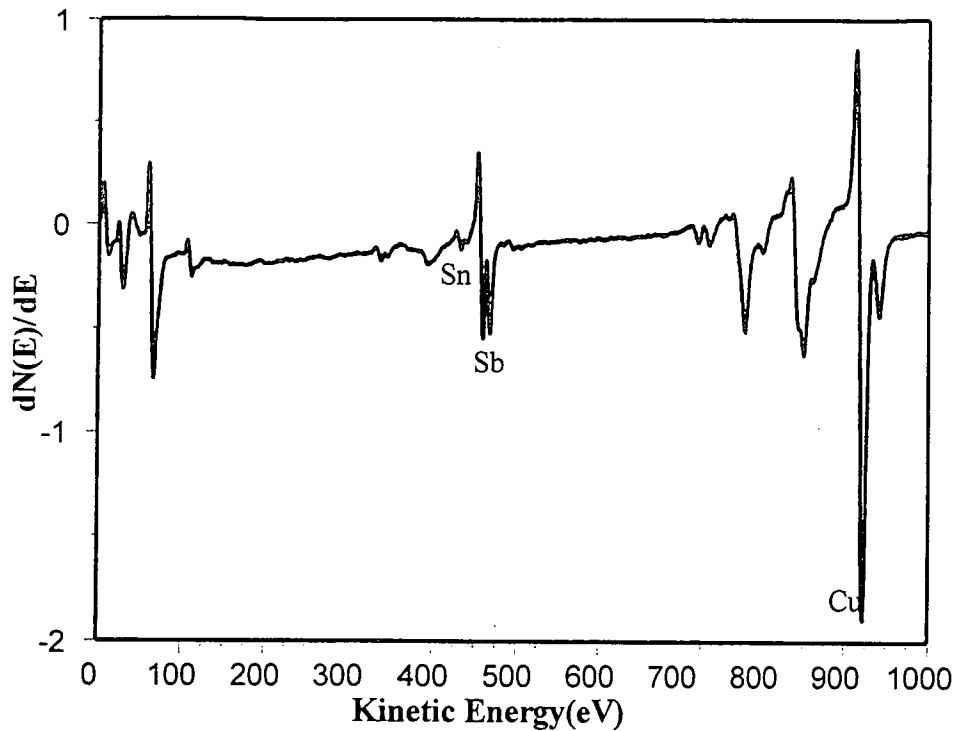


Figure 5.6 A typical Auger spectrum of the sample surface at 625 °C, taken after a LTR run. The only elements present are Cu, Sn and Sb.

## 5.5 Segregation profile divided into four regions

The Darken model calculations of segregation profiles of Sn and Sb in Cu(111) at heating rate of 0.1 K/s are shown in the **Figure 5.7**. The profiles are divided into four regions: **A**, **B**, **C** and **D**.

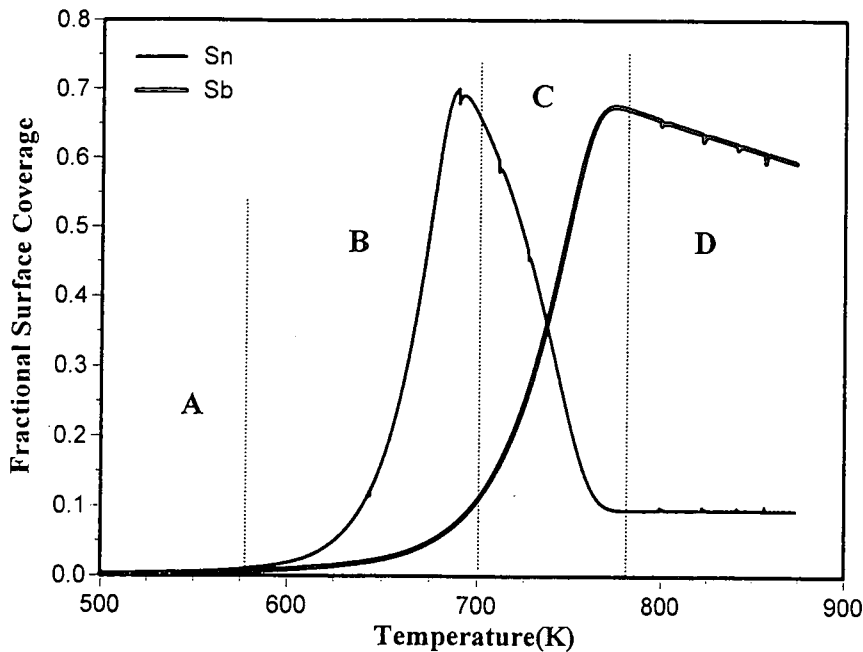


Figure 5.7 Shows the increase in surface coverage as a function of temperature for

$\alpha = 0.10$  K/s, and segregation parameters:

$$D_o(\text{Sn}) = 1.5 \times 10^{-5} \text{ m}^2 \text{ s}^{-1} \text{ and } D_o(\text{Sb}) = 1.5 \times 10^{-8} \text{ m}^2 \text{ s}^{-1},$$

$$E(\text{Sn}) = 170 \text{ kJ/mol and } E(\text{Sb}) = 150 \text{ kJ/mol},$$

$$\Delta G_{\text{Sn}} = -58 \text{ kJ/mol and } \Delta G_{\text{Sb}} = -74 \text{ kJ/mol},$$

$$\Omega_{\text{SnCu}} = -7.94 \text{ kJ/mol}, \Omega_{\text{SbCu}} = -17.5 \text{ kJ/mol and } \Omega_{\text{SnSb}} = 3.5 \text{ kJ/mol}.$$

In region A, the temperature is low and therefore the diffusion coefficient  $D$  is small. There are no detectable Sn and Sb segregation to the surface of the Cu substrate. As the temperature increases, the  $D$  values of the segregating species increase as well as the flux of atoms from the bulk to the surface. These occurrences give the profiles, as in region B. At higher temperatures, Sn, because of its higher mobility (also higher diffusion coefficient  $D$ ) than the other segregating species, Sb, attains its maximum surface coverage first. As a

result of the interaction between the atoms of the three elements (Cu, Sn and Sb in the ternary alloy system), coupled with the fact that the segregation energy of Sb is greater than that of Sn, (see **Table 5.1**) the Sn begins to desegregate as the temperature increases further and the former, (Sb), sequentially displaces it from the surface in the region C.

The Sb segregating species attains its maximum coverage and further increase in temperature leads to a decrease in its surface coverage in region D, which shows desegregation. The Sb profile in the region D, therefore obeys equilibrium segregation equations 2.46 to 2.49. After desegregating to a minimum value, Sn acquires equilibrium coverage in region D. Sn segregation profile in region D also obeys equations 2.46 to 2.49.

## 5.6 The segregation results of Sn and Sb in Cu(111)

Four Linear Temperature Ramp (LTR) runs were done by heating the ternary alloy linearly with time for heating rates of 0.05 K/s, 0.10 K/s, 0.15 K/s and 0.20 K/s. The results were also used as fitting parameters in one Constant Temperature run at 400 °C.

### 5.6.1 The LTR runs at the various heating rates.

The results are given in graphical form. On each graph, the experimental as well as the Darken's model calculations are given.

## 5.6.1.1 The LTR run at heating rate of 0.05 K/s.

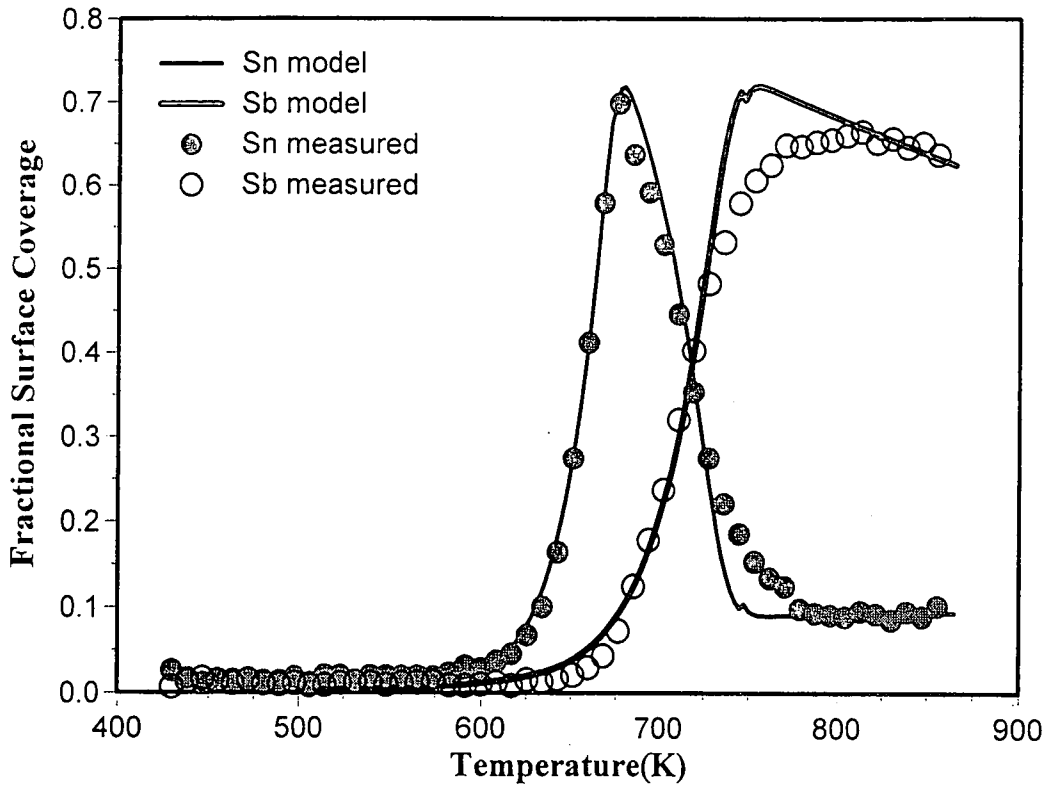


Figure 5.8 The segregation profiles of Sn and Sb in a LTR run at 0.05 K/s. The Darken model calculations are solid curves. The experimental (measured) values are given as dots.  $\alpha = 0.05$  K/s, and segregation parameters:

$$D_o(\text{Sn}) = 1.25 \times 10^{-5} \text{ m}^2 \text{ s}^{-1} \text{ and } D_o(\text{Sb}) = 2.0 \times 10^{-8} \text{ m}^2 \text{ s}^{-1},$$

$$E(\text{Sn}) = 170 \text{ kJ/mol and } E(\text{Sb}) = 150 \text{ kJ/mol},$$

$$\Delta G_{\text{Sn}} = -60 \text{ kJ/mol and } \Delta G_{\text{Sb}} = -75.4 \text{ kJ/mol},$$

$$\Omega_{\text{SnCu}} = -8.2 \text{ kJ/mol}, \Omega_{\text{SbCu}} = -17.2 \text{ kJ/mol and } \Omega_{\text{SnSb}} = 4.7 \text{ kJ/mol}.$$

## 5.6.1.2 The LTR run at heating rate of 0.10 K/s.

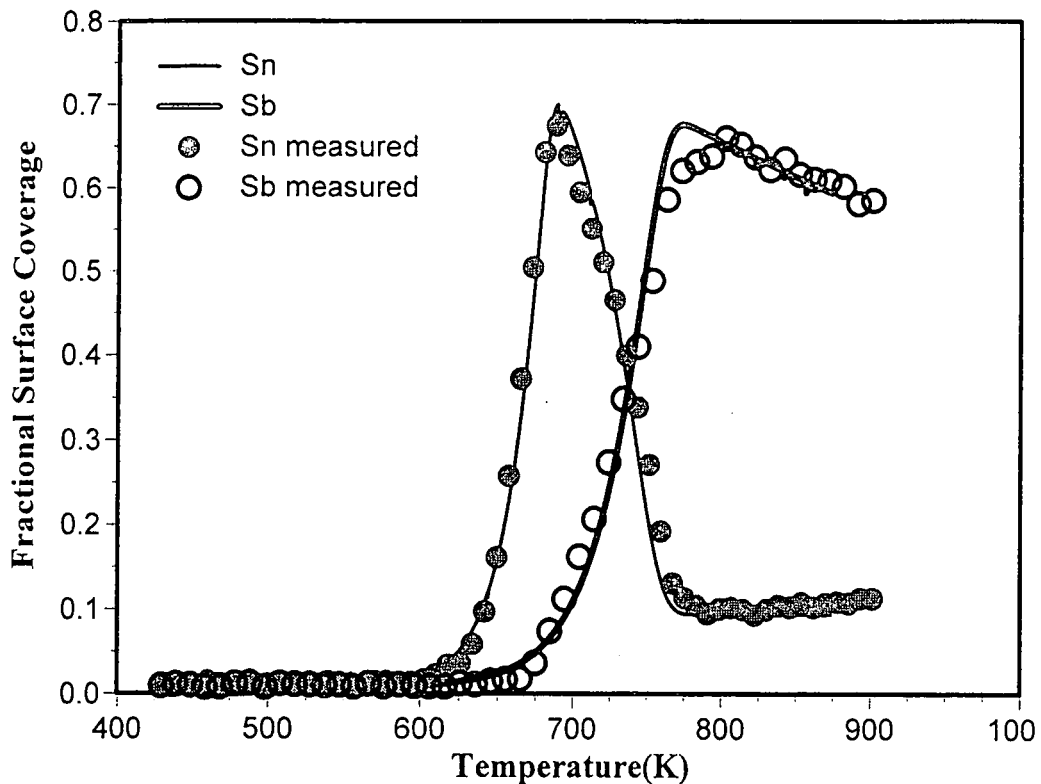


Figure 5.9 The segregation profiles of Sn and Sb in a LTR run at 0.10 K/s. The Darken model calculations are solid curves. The experimental (measured) values are given as dots.  $\alpha = 0.10$  K/s, and segregation parameters:

$$D_o(\text{Sn}) = 1.5 \times 10^{-5} \text{ m}^2 \text{ s}^{-1} \text{ and } D_o(\text{Sb}) = 1.9 \times 10^{-8} \text{ m}^2 \text{ s}^{-1},$$

$$E(\text{Sn}) = 170 \text{ kJ/mol and } E(\text{Sb}) = 150 \text{ kJ/mol},$$

$$\Delta G_{\text{Sn}} = -58 \text{ kJ/mol and } \Delta G_{\text{Sb}} = -74 \text{ kJ/mol},$$

$$\Omega_{\text{SnCu}} = -7.9 \text{ kJ/mol}, \Omega_{\text{SbCu}} = -17.5 \text{ kJ/mol and } \Omega_{\text{SnSb}} = 3.5 \text{ kJ/mol}.$$

## 5.6.1.3 The LTR run at heating rate of 0.15 K/s.

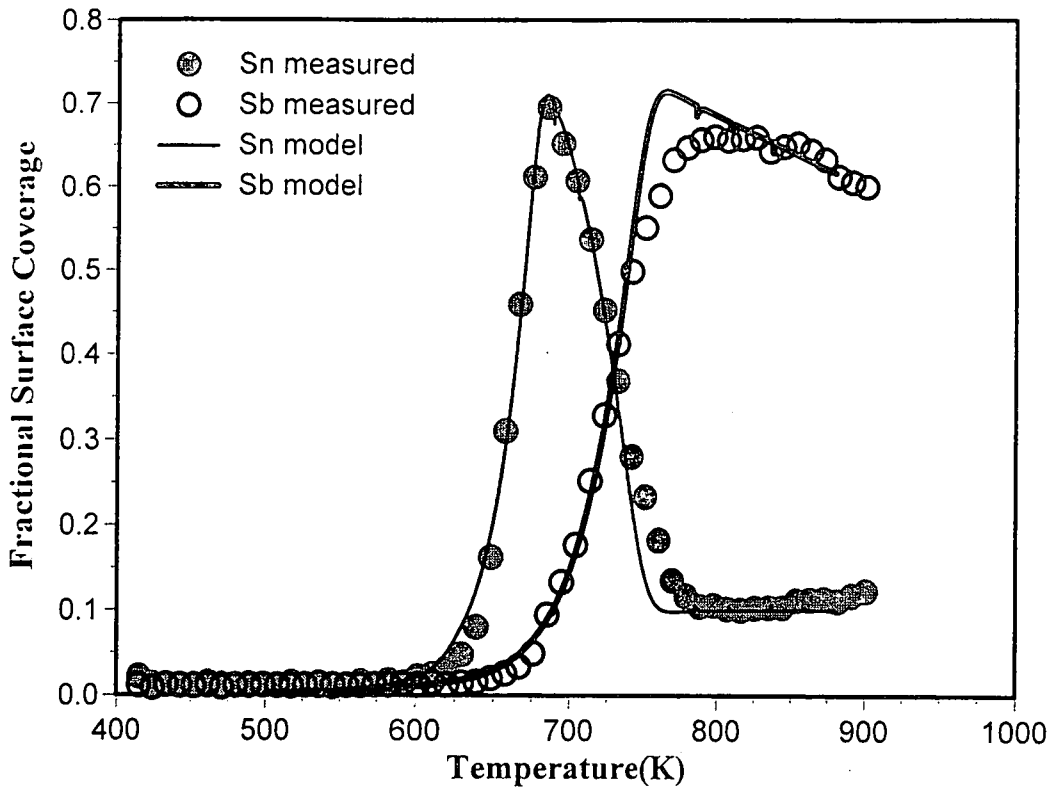


Figure 5.10 The segregation profiles of Sn and Sb in a LTR run at 0.15 K/s. The Darken model calculations are solid curves. The experimental (measured) values are given as dots.  $\alpha = 0.15$  K/s, and segregation parameters:

$$D_o(\text{Sn}) = 2.80 \times 10^{-5} \text{ m}^2 \text{ s}^{-1} \text{ and } D_o(\text{Sb}) = 1.9 \times 10^{-8} \text{ m}^2 \text{ s}^{-1},$$

$$E(\text{Sn}) = 170 \text{ kJ/mol and } E(\text{Sb}) = 150 \text{ kJ/mol},$$

$$\Delta G_{\text{Sn}} = -58 \text{ kJ/mol and } \Delta G_{\text{Sb}} = -75 \text{ kJ/mol},$$

$$\Omega_{\text{SnCu}} = -9.0 \text{ kJ/mol}, \Omega_{\text{SbCu}} = -16.5 \text{ kJ/mol and } \Omega_{\text{SnSb}} = 2.8 \text{ kJ/mol}.$$



## 5.6.1.4 The LTR run at heating rate 0.20 K/s.

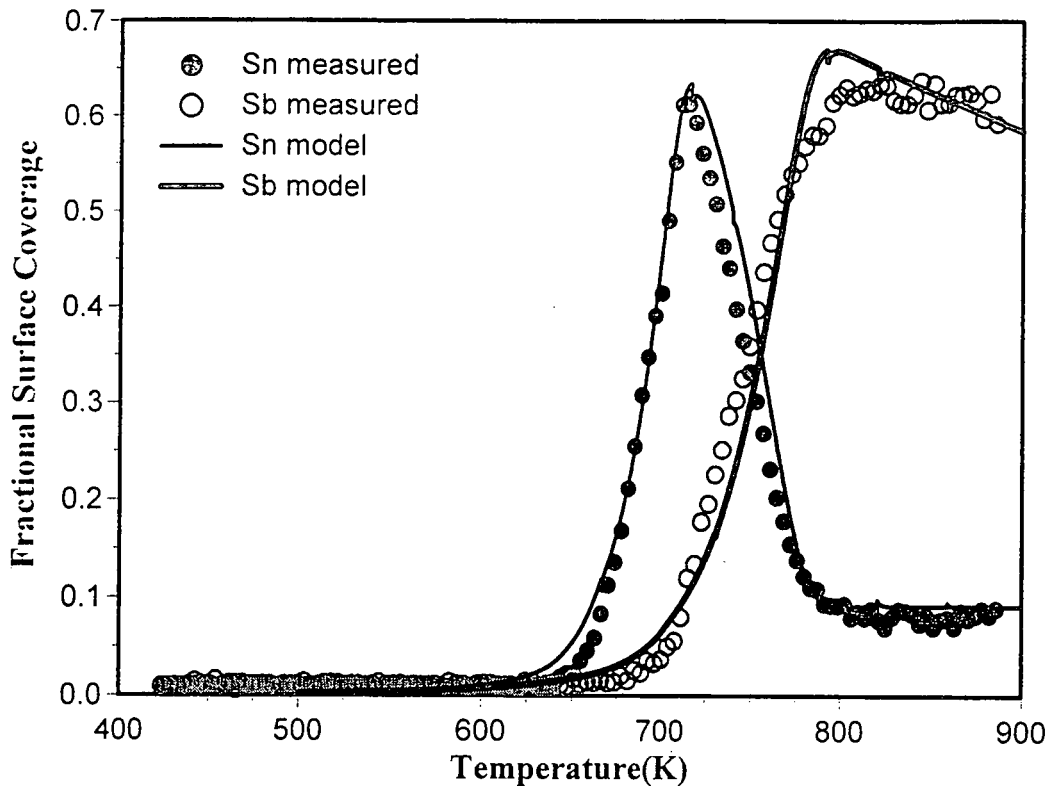


Figure 5.11 The segregation profiles of Sn and Sb in a LTR run at 0.20 K/s. The Darken model calculations are solid curves. The experimental (measured) values are given as dots.  $\alpha = 0.20$  K/s, and segregation parameters:

$$D_o(\text{Sn}) = 8.0 \times 10^{-6} \text{ m}^2 \text{ s}^{-1} \text{ and } D_o(\text{Sb}) = 1.9 \times 10^{-8} \text{ m}^2 \text{ s}^{-1}$$

$$E(\text{Sn}) = 170 \text{ kJ/mol and } E(\text{Sb}) = 150 \text{ kJ/mol,}$$

$$\Delta G_{\text{Sn}} = -58 \text{ kJ/mol and } \Delta G_{\text{Sb}} = -74 \text{ kJ/mol,}$$

$$\Omega_{\text{SnCu}} = -7.94 \text{ kJ/mol, } \Omega_{\text{SbCu}} = -17.0 \text{ kJ/mol and } \Omega_{\text{SnSb}} = 3.5 \text{ kJ/mol.}$$

In all the LTR runs, the comparisons between the experimental values and the model calculations show reasonable agreement in all the heating rates considered. There is some difference, however between the measured and calculated values in the profiles;

particularly, in the region just before Sb reaches a maximum. This may be due to the restriction in the number of layers used during the calculations. Increasing the number of layers might result in a better fit. But this will increase the calculating time a great deal. Already it takes eight hours on a 550 MHz computer to calculate one segregation profile.

It can also be seen that Sn was the first to segregate to the surface despite the fact that its bulk concentration (0.133 at. %) is higher than Sb (0.180 at. %). This confirms the fact that Sn mobility is higher than Sb. The rapidly segregating Sn, however, is displaced from the surface by the slower but stronger segregating Sb. The desegregating rate of Sn is determined by the segregation rate of Sb; the desegregation process is "normally" slower than that of segregation. There is a small decrease in Sb kinetics because of the presence of Sn on the surface. The equilibrium segregation profile of Sb looks like that of the Cu-Sb binary alloy [86].

### 5.6.2 A Constant Temperature Run at 400 °C

The modified Darken model was also used to fit the segregation profile obtained for a constant temperature run at 400 °C. The results are shown in **Figure 5.12**.

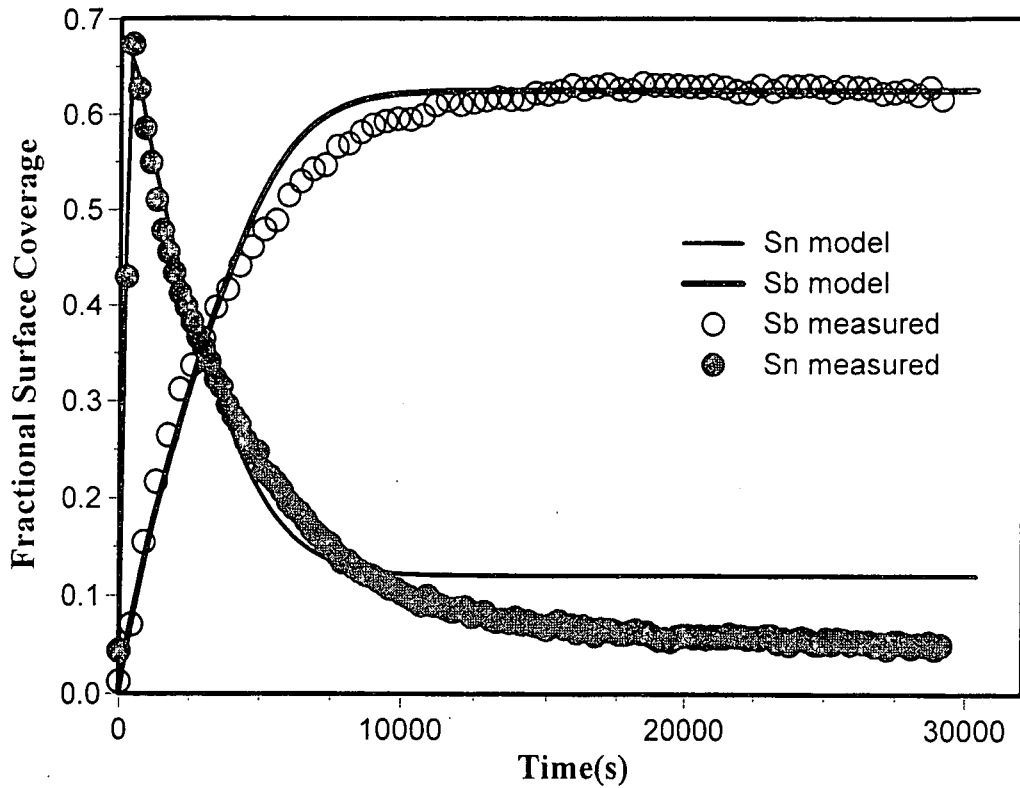


Figure 5.12 Shows the increase in surface coverage as a function of time for constant temperature of 400 °C and segregation parameters:

$$D_o(\text{Sn}) = 1.58 \times 10^{-5} \text{ m}^2 \text{ s}^{-1} \text{ and } D_o(\text{Sb}) = 1.93 \times 10^{-8} \text{ m}^2 \text{ s}^{-1},$$

$$E(\text{Sn}) = 170 \text{ kJ/mol and } E(\text{Sb}) = 150 \text{ kJ/mol},$$

$$\Delta G_{\text{Sn}} = -55.5 \text{ kJ/mol and } \Delta G_{\text{Sb}} = -69.25 \text{ kJ/mol},$$

$$\Omega_{\text{SnCu}} = -8.2 \text{ kJ/mol}, \Omega_{\text{SbCu}} = -20 \text{ kJ/mol and } \Omega_{\text{SnSb}} = 5.0 \text{ kJ/mol}.$$

The good fit obtained with the segregation parameters very close to the parameters for the LTR runs acknowledge the applicability of the model. See Tables 5.1 and 5.2.

## 5.6.3 Summary of segregation parameters

The segregation parameters are summarised in Tables 5.1 and 5.2 below.

	Property	( $E$ ) Activation Energy (kJ/mol)	( $D_0$ ) Pre-exponential factor ( $m^2/s$ )	$\Delta G$ Segregation Energy (kJ/mol)
Sn	LTR 0.05 K/s	170	$1.25 \times 10^{-5}$	-60.0
	LTR 0.10 K/s	170	$1.50 \times 10^{-5}$	-58.0
	LTR 0.15 K/s	170	$2.80 \times 10^{-5}$	-60.0
	LTR 0.20 K/s	170	$0.80 \times 10^{-5}$	-58.0
	Const. Temp. 400 °C	170	$1.58 \times 10^{-5}$	-55.5
Sb	LTR 0.05 K/s	150	$2.00 \times 10^{-8}$	-75.40
	LTR 0.10 K/s	150	$1.90 \times 10^{-8}$	-74.00
	LTR 0.15 K/s	150	$1.90 \times 10^{-8}$	-75.00
	LTR 0.20 K/s	150	$1.90 \times 10^{-8}$	-74.00
	Const. Temp. 400 °C	150	$1.93 \times 10^{-8}$	-69.25

Table 5.1 A summary of the segregation parameters

Interaction coefficient(kJ/mol)	LTR				Const. Temp. 400 °C
	0.05 K/s	0.10 K/s	0.15 K/s	0.20 K/s	
$\Omega_{SnSb}$	4.7	3.5	2.8	3.5	5.0
$\Omega_{SnCu}$	-8.2	-7.9	-9.0	-7.9	-8.2
$\Omega_{SbCu}$	-17.2	-17.5	-16.5	-17.0	-20.0

**Table 5.2** The interaction parameters for Cu(111), Sn, Sb

The results indicate the repeatability of the segregation parameters at different heating rates, further confirming the advantage in the use of the LTR technique, viz., that segregation parameters can be obtained from one experimental run.

## 5.7 A General Discussion

### 5.7.1 The segregation profiles for different heating rates

A nice trend evolves when the segregation profiles for the different heating rates are put together. The shape of the profiles for both Sn and Sb remain the same. However, their maximum surface coverage change for the different heating rates. The presentation is shown below in **Figure 5.13**.

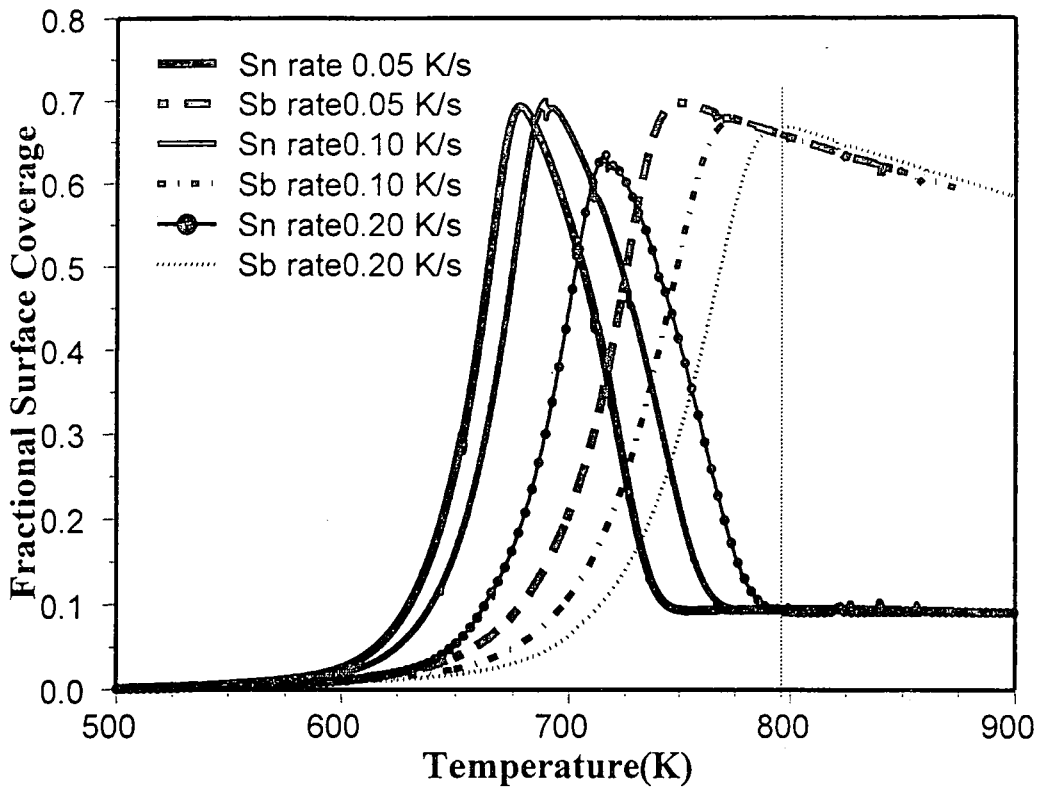


**Figure 5.13** The segregation profiles of Sn and Sb pairs at different sample heating rates of: 0.05 K/s, 0.10 K/s and 0.20 K/s. The profiles shift to the right for increasing heating rates. Also, the maximum coverage of both Sn and Sb decrease with increasing heating rate.

At low heating rates, a long time is spent at a specific temperature and the atoms have ample opportunity to segregate to the surface. An increase in the heating rate leads to a decrease in the time spent at a temperature and therefore a decrease in the amount of dissolved atoms that will segregate to the surface. This implies that an increase in the surface coverage would appear at a lower temperature for lower heating rates.

The same can be said for the maximum coverage of Sn. It decreases with increasing heating rate. It is also clear that once the equilibrium coverage are reached ( $\sim 800$  K), the profile is not dependent on the heating rate.

### 5.7.2 The influence of the interaction energies between the different atoms.

#### 5.7.2.1 Change in the interaction coefficient between Sn and Sb atoms ( $\Omega_{SnSb}$ ).

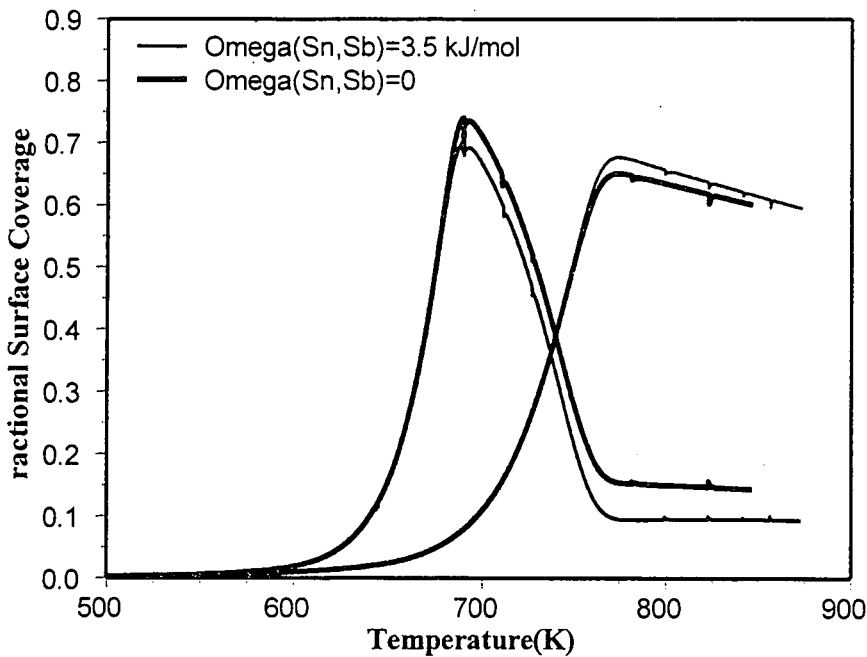


**Figure 5.14** Change in the interaction coefficient between Sn and Sb. Thick solid curves represent no interaction between Sn and Cu atoms. The light solid curves are the experimental fit curves. LTR run at 0.10 K/s heating rate parameters were used. (See Table 5.1 and 5.2).

The experimental results show there is repulsive interaction between Sn and Sb atoms, and the repulsive interaction energy is 3.5 kJ/mol. On the other hand, when the interaction coefficient is zero, model calculations for both Sn-Sb profile pair (thick solid curve) deviate significantly from experimental values (light solid curve). A slightly higher Sn maximum coverage and lower Sb maximum coverage is shown.

A further indication of the repulsive interaction is observed during the desegregation of Sb. In this part of the curve where the concentration of Sb decreases, there is, although small, an increase in the Sn coverage.

### 5.7.2.2 Change in the interaction coefficient between Sn and Cu atoms ( $\Omega_{SnCu}$ ).

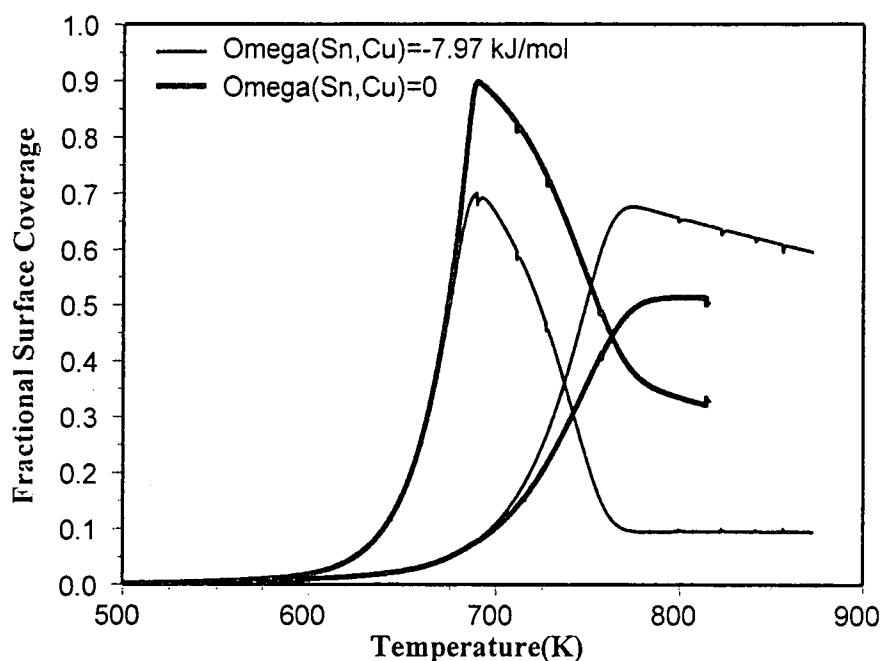
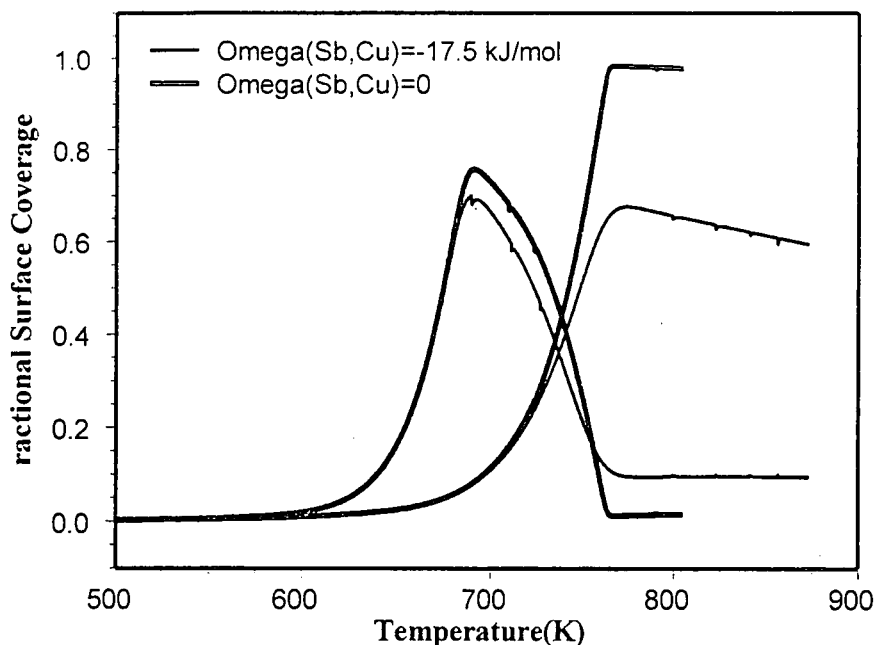


Figure 5.15 Change in the interaction coefficient between Sn and Cu. Thick solid curves represent no interaction between Sn and Cu atoms. The light solid curves are the experimental fit curves.

The experimental results show there is attractive interaction between Sn and Cu atoms and the interaction energy is  $-7.94 \text{ kJ/mol}$ . This could lead to compound formation. On the other hand, when the interaction coefficient is zero, model calculations for both Sn-Sb profile pair (thick solid curve) deviate significantly from experimental values (light solid curve). Again, it can also be deduced from the figure that the maximum coverage of Sn is eventually determined by this attractive interaction energy between the Sn and Cu atoms.



### 5.7.2.3 Change in the interaction coefficient between Sb and Cu atoms ( $\Omega_{SbCu}$ ).



**Figure 5.16** Change in the interaction coefficient between Sb and Cu. Thick solid curves represent no interaction between Sb and Cu atoms. The light solid curves are the experimental fit curves.

The experimental results show there is attractive interaction between Sb and Cu atoms and the interaction energy is  $-17.5$  kJ/mol. This also influences the maximum Sn coverage on the Cu substrate. This could also lead to compound formation between the atoms of Sb and Cu. On the other hand, when the interaction coefficient is zero, model calculations for both the Sn and Sb segregation profiles (thick solid curve) deviate significantly from experimental values (light solid curve).

The equilibrium coverage for Sb can be said to be due to its high segregation energy and an attractive interaction with Cu atoms; therefore a preference for unlike first neighbour bonds between Sb and Cu atoms.

A higher rate of change in the surface coverage near equilibrium is due to a repulsive interaction between Sn and Sb (tendency for cluster formation).

## 5.8 Comparison to the Cu-Sn and Cu-Sb binary systems

At this stage, not much work has been done in the study of ternary systems. However, some works on binary systems have been done for Cu-Sn and Cu-Sb alloys. Although the two systems are completely different from each other, mainly on the account of the existence of interaction between the different atoms, an attempt is being made to compare some of the common parameters that have been reported with that of the present work. Table 5.3 shows the comparisons.

	Method	Bulk Concentration at.%	$D_o$ ( $m^2s^{-1}$ )	$E$ (kJ/mol)	$\Delta G$ (kJ/mol)	Reference
Sn	Surface Segregation	0.12	$(7\pm 6)\times 10^{-6}$	168 $\pm$ 5	-76 $\pm$ 3	[28]
	Sn <sup>113</sup> tracer	-	$1.1\times 10^{-5}$	189	-	[84]
	Surface Segregation	0.5	$2.0\times 10^{-6}$	176	-67	[70]
	LTR	0.1	$9.2\times 10^{-4}$	189	-	[85]
	LTR	0.133(Sb-0.18)	$1.58\times 10^{-5}$	170	-58	Present work

Table 5.3 (a) Comparison of measured segregation parameters (Sn).

Sb	LTR	0.18	$6.6 \times 10^{-7}$	177	-77	[86]
	Sb <sup>124</sup> tracer	-	$3.4 \times 10^{-5}$	176	-	[87]
	LTR	0.18(Sn-0.133)	$2.6 \times 10^{-8}$	150	-74	Present work

**Table 5.3 (b)** Comparison of measured segregation parameters (Sb).

In Table 5.3 (a) and (b) the segregation parameters (the diffusion parameters) compare favourably with the results from other work. The lower segregation energy of Sn in the ternary alloy can be expected as a result of the stronger competing Sb and the fact that there is repulsive interaction between the atoms of the two segregates.

From the results in this work, there are definite attractive interactions between Sn and Cu as well as between Sb and Cu. Although one would expect the same results for the binary systems, these attractive interactions were not observed [85-86]. The reason for this is not clear.

## 5.9 Significance of the corrected APPH technique

Notwithstanding the small difference in the segregation profiles of corrected and measured APPH's values as seen in Figure 5.3, as a result of better choice of the energy regions for Sn and Sb, the segregation parameters are influenced if the measured values are not corrected in the quantification. Table 5.4 shows the significant difference between the two; the measured and the corrected.

Parameter	Corrected	Measured	% difference
$\Delta G(\text{Sn})$	-58.0	-57.7	0.5
$\Delta G(\text{Sb})$	-74.0	-72.2	2.5
$\Omega_{\text{SnSb}}$	3.5	3.1	10.3
$\Omega_{\text{SnCu}}$	-7.94	-6.38	19.7
$\Omega_{\text{SbCu}}$	-17.0	-15.0	11.5

**Table 5.4** Comparison between corrected and measured segregation parameters for 0.20 K/s rate.

The above results have validated the technique of extracting the true Auger yield contributions for each segregate (as a result of the overlapping of peaks) from the combined APPH.

# CHAPTER SIX

## CONCLUSION

The LTR technique, which has been used mainly in the study of binary alloy system, has successfully been extended, in this study, to the ternary alloy system. In the process, the segregation parameters of Sn and Sb in a Cu(111) single crystal have been determined. Again, it has been confirmed that segregation parameters can be extracted from a single experimental run at some heating rate.

A LTR run gives both the kinetic and equilibrium segregation profile of a segregate. As a result, the equilibrium segregation equations were used mathematically to get the segregation energies ( $\Delta G_i$ ) and the various interaction energy parameters ( $\Omega_{ij}$ ). The modified Darken equations, which account for both the kinetic and equilibrium segregation profiles, were then solved using the segregation parameters as the fit values. It can also be said that the Darken model computer program that has been used for binary systems has been extended successfully to that of ternary systems. The results of the Darken calculations simulated the experimental data amazingly well and confirmed the applicability of the model.

In refining the quantification of the APPH, a unique technique has been developed in this study that enables the contribution of each segregate to be extracted from the measured, overlapping, APPH's. The problem of a "bad" choice of energy regions for the APPH measurement of a particular element as a result of peak overlapping with a second element, has been resolved.

The sequential segregation profiles of Sn and Sb could be explained satisfactorily in terms of the difference in their mobilities and segregation energies as well as in the interaction energies between Sn, Sb and Cu atoms.

Finally, the values of the segregation parameters for Sn and Sb segregates in Cu(111),  $\Delta G_{Sn}$ ,  $\Delta G_{Sb}$ ,  $\Omega_{SnSb}$ ,  $\Omega_{SnCu}$ ,  $\Omega_{SbCu}$ ,  $D_o(Sn)$ ,  $D_o(Sb)$ ,  $E_{Sn}$  and  $E_{Sb}$ , are summarised in Table 6.1 below.

Parameter	Sn	Sb
$\Delta G$ (kJ/mol)	$-59 \pm 1$	$-74.6 \pm 0.7$
$D_o$ (m <sup>2</sup> /s)	$(1.58 \pm 0.90) \times 10^{-5}$	$(1.93 \pm 0.50) \times 10^{-8}$
$E$ (kJ/mol)	170	150
$\Omega_{SnSb}$ (kJ/mol)	$3.62 \pm 0.80$	
$\Omega_{SnCu}$ (kJ/mol)	$-8.25 \pm 0.50$	
$\Omega_{SbCu}$ (kJ/mol)	$-17.05 \pm 0.40$	

Table 6.1 The average segregation parameters of the segregates Sn and Sb in Cu(111).

## 6.1 What has evolved in the course of this work

1. In July 1999, at South African Institute of Physics (SAIP) annual conference at the University of Port Elizabeth, a presentation was given entitled:  
“Linear Programmed Heating applied to Ternary Alloys—Preliminary Calculations”.  
Authors: Asante JKO; Terblans JJ; Du Plessis J; Roos WD.
2. In July 2000, at the Rand Afrikaans University in Johannesburg, two posters of the work were presented again at SAIP annual conference.  
Poster number 1 was entitled:  
“Co-segregation in a Cu(111),Sn,Sb ternary single crystal”.  
Authors: Asante JKO; Roos WD; Du Plessis J; Terblans JJ.  
Provisional results of the present work were given.  
Poster number 2 was entitled:  
“Extracting Auger Yield Contributions From The Combined Peak To Peak Height Of Overlapping Peaks Using Only The Spectra Of The Standards”  
Authors: Asante JKO; Maritz MF; Roos WD.
3. An article on the Poster number 2. entitled, “Quantification from Overlapping Auger Peak-to-peak Heights”, has already been submitted for publication in *Surf. Inter. Anal.*
4. Another article on the experimental work (Poster number 2) is in preparation.
5. APSIAC. 2000. Beijing China. October 2000. The two posters were presented.  
Poster 1: “Co-segregation in a Cu(111),Sn,Sb ternary single crystal”.  
Poster 2: “Extracting Auger Yield Contributions From The Combined Peak To Peak Height Of Overlapping Peaks Using Only The Spectra Of The Standards”

## 6.2 Future work

The success of this work opens up segregation studies on ternary systems.

Further work on the ternary systems Cu(100) and Cu(110) substrate using the segregates Sn, Ag and Sb are envisaged in the near future. In addition, work will have to be done to get "smarter" algorithms whereby computer calculating time would be decreased. This would imply increasing the number of layers for better fits.



# APPENDIX

## Matlab programme for APPH correction of overlapping peaks

---

% The Apph-function

function Y=apph(I)

Y=max(I)-min(I);

---

% The function to be minimized

function x=apphres(a, IA1,IA2, IB1, IB2, b)

Y1=a(1)\*IA1+a(2)\*IB1;

Y2=a(1)\*IA2+a(2)\*IB2;

S1=apph(Y1);

S2=apph(Y2);

x=(S1-b(1))^2 + (S2-b(2))^2;

---

% Script file for computing the Sn and Sb contribution to the yield.

% The measured APPH's are stored as two columns in XX and the time

% as a column in TIME.

% The spectrum of the Sn standard over the first interval is stored in

% IA1 and that of Sb over the first interval in IB1. Similarly the

% standards over the second interval, are stored in IA2 and IB2

```

% respectively. IA1, IA2, IB1 and IB2 are all column vectors.
% The spectra of the standards over the whole energy range are stored
% as columns in SnSTD and SbSTD respectively.

CC=[ ]; % Create an empty matrix
OPT(2)=0.001; OPT(3)=0.001; % Tolerance parameters for fmins routine
a=[1 0]; % Initial guess for the first timestep
for k=1: length(XX) % Loop through all timesteps
    b=XX(k,:); % Select the k-th measured APPH's
    a=fmins('apphes',a, OPT, [ ], IA1, IA2, IB1, IB2, b);
    % Solve nonlinear system
CC=[CC; a]; % Store result in CC matrix
end % End of loop

sca1=apph(SnSTD); % Scaling factor of Sn standard
sca2=apph(SbSTD); % Scaling factor of Sb standard
CCO(:,1)=XX(:,1)/sca1; % Coarse estimate of Sn contribution
CCO(:,2)=XX(:,2)/sca2; % Coarse estimate of Sb contribution
hold off; plot(TIME,CC, 'r'); % Plot correct contributions in red solid
hold off; plot(TIME,CCO, 'b'); % Plot coarse estimate in blue dotted

```

---

## BIBLIOGRAPHY

1. C. Uebing, H. Viefhaus and H.J. Grabke, *Appl. Surf. Sci.*, **32**, 1988, 363.
2. S. Hofman, *Scan. Electron. Microsc.*, **3**, 1985, 1071.
3. E.C. Viljoen and J. du Plessis, *Surf. Sci.* **431**, 1999, 128.
4. J.W. Gibbs: *The Scientific Papers of J.W. Gibbs*, **1**, Dover, New York, 1961, 219.
5. A. Rodnyansky, Y.J. Warburton and L.D. Hanke, *Surf. Inter. Anal.* **29**, 2000, 215.
6. C. Uebing, H. Viefhaus and H.J. Grabke: *Surface Segregation and Related Phenomena*, Eds. P. Dowben and A. Miller, CRC Press, Boca Raton, Fl, 1990, 241.
7. H. Viefhaus, J. Peters and H.J. Grabke, *Surf. Inter. Anal.* **10**, 1987, 280.
8. C. Uebing, *Surf. Sci.* **225**, 1990, 97.
9. C. Uebing, H. Viefhaus and H.J. Grabke, *Surf. Sci.* **264**, 1992, 114.
10. C. Uebing and H. Viefhaus, *Surf. Sci.* **236**, 1990, 29.
11. D.M. Zehner and D.W. Goodman, Eds., *Physical and Chemical Properties of Thin Metal Overlayers and Alloy Surfaces*, Materials Research Society, Pittsburgh, PA, 1987.
12. M. P. Seah, *Surf. Sci.*, **53**, 1975, 68.
13. F. M. d'Heurle and A. Gangulee, *The Nature and behaviour of Grain Boundaries* H. Hu, Ed., Plenum Press, New York, 1972, 339.
14. D. Gupta, *Metall. Trans.*, **8A**, 1977, 1431.
15. W.C. Johnson and D.F. Stein, *J. Amer. Ceram. Soc.*, **58**, 1975, 485.
16. R.M. Latanision and Opperhauser, Jr., *Metall. Trans.*, **5**, 1974, 483.
17. S. Dinda and W.R. Warke, *Mat. Sci. Eng.*, **24**, 1976, 199.
18. C.G. Munger, *Corrosion Prevention by Protective Coatings*, NACE, 1984, 130-131.
19. G.R. Conner, *Appl. Surf. Anal.*, ASTM STP, **699**, 1980, 54.
20. H.J. Grabke, W. Paulitschke, G. Tauber and H. Viefhaus, *Surf. Sci.*, **377**, 1977, 63.

21. H.J. Grabke, Mater. Sci. Eng., **91**, 1980, 42.
22. C. Lea and B. Roebuck, Met. Sci., **262**, 1981, 15.
23. J.H. Sinfelt, Advan. Catal., **23**, 1973, 91.
24. C.R. Helm and J. H. Sinfelt, Surf. Sci., **72**, 1978, 229.
25. J. Y. Wang, Ph.D. Thesis, University of the Orange Free State, South Africa, 1997.
26. D. McLean, *Grain Boundaries in Metals*, Oxford University Press, Oxford, 1957.
27. M. Guttman, Surf. Sci., **201**, 1988, L519.
28. E.C. Viljoen and J. du Plessis, Surf. Inter. Anal., **23**, 1995, 110.
29. J.Y. Wang et al., Surf. Sci., **423**, 1999, 16.
30. M. Harzl and M. Leisch, Appl. Surf. Sci., 1999, 145.
31. E. Clauberg, C. Uebing and H.J. Grabke, Appl. Surf. Sci., 1999, 143.
32. Z.M. Jiang et al., Thin Sol. Films, 1999, 336.
33. M. Gutmann, Surf. Sci. **53**, 1975, 213.
34. Ch. Muller, Ch. Uebing, M. Kottcke, Ch. Rath, L. Hammer, and K Heinz, Surf. Sci., **400**, 1998, 87.
35. B. Eltester and C Uebing, Surf. Sci., **347**, 1996, 39.
36. M. Militzer, Yu N. Ivashchenko, A.V. Krajnikov et al., Surf.Sci. **261**, 1992, 267.
37. F. S. Honey, G. Bozzolo and B. Good, Appl. Surf. Sci. **137**, 1999, 157.
38. J.M.Chen, T.S. Sun et al. J. Vac. Sci. Tech. **15(2)**, 1978, 470.
39. P.Dumoulin and M.Guttman, Mater. Sci. Eng., **42**, 1980, 249.
40. M.M. Eisl, B.M. Reichl and H. Stori, Surf. Sci., **336**, 1995, 377
41. M.P. Seah and C. Lea, Philos. Mag., **627**, 1975, 31.
42. <http://members.aol.com/pewtrsocety/glossy.htm>
43. <http://users.michiana.org/rosses/babbit.html>
44. <http://www.connector.org/timecompounds03.html>
45. <http://www.connector.org/coppertin03.html>
46. J. du Plessis and E.C. Viljoen, Appl. Surf. Sci., **59**, 1992, 171.
47. J. du Plessis, *Surface Segregation*, Diffusion and Defect Data Vol. 11, Sci-Tech Pub. Ltd., 9, 1990, 125.

48. J. du Plessis and P.E. Viljoen, Surf. Sci. Let., **276**, 1992, L7.
49. G.N. van Wyk, J. du Plessis and E. Taglauer, Surf. Sci., **255**, 1991, 73.
50. J. du Plessis, Applied Surf. Sci., 70/71, **303**, 1993, 307.
51. S. Hofman and J. Erlewein, Surf. Sci., **77**, 1978, 591.
52. A.D Brailsford, Surf. Sci., **94**, 1980, 387.
53. J. du Plessis and G.N. Van Wyk, J. Phys. Chem. Solids, **50**, 1989, 237.
54. M. Menyhard, Surf. Interf. Anal. **19**, 1992, 615.
55. M. M. Eisl, B.M. Reichl and H. Stori, Applied Surf. Sci., 70/71, 1993, 137.
56. M. Guttman, Surf. Sci. **53**, 1975, 216.
57. J.H. Hildebrand and R.L. Scott *The Solubility of Nonelectrolytes*, 3<sup>rd</sup> ed., Van Nostrand Reinhold, New York, 1950.
58. C.H.P. Lupis, *Chemical Thermodynamics of Materials*, North-Holland, Amsterdam, 1983.
59. C. J. McMahan, Jr and L. Marchut, J. Vac. Sci. Technol., **15(2)**, 1978, 456.
60. J. du Plessis and G. N. Van Wyk, J. Phys. Chem. Solids, **49**, 1988, 1442.
61. J. du Plessis and E.C. Viljoen, Appl. Surf. Sci. **100/101**, 1996, 222.
62. L.S. Darken, Trans. AIME **180**, 1949, 430.
63. J. du Plessis, *Surface Segregation*, Diffusion and Defect Data Vol.11, Sci-Tech Pub. Ltd., **9**, 1990, 70.
64. [http://www.chem.qmw.ac.uk/surfaces/scc/scat5\\_2.htm](http://www.chem.qmw.ac.uk/surfaces/scc/scat5_2.htm).
65. <http://www.chips.ibm.com/services/asweb03.html>.
66. Material-Technologie & Kristalle, Büro für Forschungsmaterialien, Karl-Heinz-Beckurts-Strasse 13, D52428, Jülich, Germany
67. Goodfellow Cambridge Limited, Cambridge CB4, 4DJ, England.
68. J. Crank, *The Mathematics of Diffusion*, 2<sup>nd</sup> edition, Clarendon, Oxford, 1975.
69. D. Briggs and M.P. Seah (Eds.), *Practical Surface Analysis by Auger and X-ray Photoelectron Spectroscopy*, Wiley, New York, 1983, 186.
70. S. Hofmann and J. Erlewein, Scripta Met., **10**, 1976, 857.
71. F.J. Mojica and L.L. Levenson, Surf. Sci., **59**, 1976, 447.
72. G.L.P. Berning and W.J. Coleman, Surf. Sci., **173**, 1986, 411.

73. S. Hofman and W. Mader, *Surf. Interf. Anal.*, **15**, 1990, 794.
74. I. Jager, *Surf. Sci.*, **366**, 1996, 166.
75. C.J. Powell, A. Jablonski, I.S. Tilinin, S. Tanuma and D.R. Penn, *J. of Electron Spec. and Related Phenomena*, **98-99**, 1999, 3.
76. S. Tanuma, C.J. Powell and D.R. Penn, *Surf. Interf. Anal.*, **17**, 1991, 911.
77. S. Tanuma, C.J. Powell and D.R. Penn, *Surf. Interf. Anal.*, **21**, 1994, 165.
78. R. Shimizu, *J. of Appl. Phys.*, **22**, 1983, 1631.
79. S. Ichimura, R. Shimizu and J.P. Langeron, *Surf. Sci.*, **124**, 1983, L49.
80. W.D. Roos, G.N. van Wyk and J. du Plessis, *J. Surf. Interf. Anal.*, **22**, 1994, 65.
81. J.M.M. Nijs and G.K.M. Aarts, *Surf. Interf. Anal.*, **17**, 1991, 628.
82. J.K.O. Asante, W.D. Roos and M.F. Maritz, Submitted for publication, (*Surf. Interf. Anal.*)
83. MATLAB, The Language of Technical Computing, Version 5, The Math Works Inc., 24 Prime Park Way, Natick, MA 01760-1500.
84. P.P. Kuzmenko, E.F. Ostrovskii and V.S. Kovalchuk, *Fiz. Tverd. Tela*, **4**, 1962, 490.
85. E.C. Viljoen and J. du Plessis, *Surf. Inter. Anal.*, **22**, 1994, 600.
86. W.J. Erasmus, MSc Thesis, University of the Orange Free State, South Africa, 1999.
87. M.C. Inman and L.W. Barr, *Acta. Met.*, **8(2)**, 1960, 112.